Dissection of Immunomodulatory Mechanisms in Chronic Lung Disease Under Various Conditions

Lee, Seunghyun

Department of Medical Science

Graduate School

Yonsei University

Dissection of Immunomodulatory Mechanisms in Chronic Lung Disease Under Various Conditions

Advisor Shin, Sung Jae

A Master's Thesis Submitted
to the Department of Medical Science
and the Committee on Graduate School
of Yonsei University in Partial Fulfillment of the
Requirements for the Degree of
Master of Medical Science

Lee, Seunghyun

June 2025

Dissection of Immunomodulatory Mechanisms in Chronic Lung Disease Under Various Conditions

This Certifies that the Master's Thesis of Lee, Seunghyun is Approved

Committee Chair	Ryu, Ji Hwan
Committee Member	Shin, Sung Jae
Committee Member	Park, Sang Chul

Department of Medical Science
Graduate School
Yonsei University
June 2025

ACKNOWLEDGEMENTS

석사 학위를 수행하는 동안 힘든 순간들도 있었지만, 그 만큼 값진 배움이 있었던 소중한 시간이었습니다. 이 과정을 무사히 마칠 수 있었던 것은 주변의 많은 분들의 격려와 따뜻한 도움 덕분이며, 저에게는 더 나은 인생을 향해 한 걸음 나아갈 수 있는 성장의 여정이었다고 생각합니다.

무엇보다 과학자로서 사고하는 법, 연구의 흐름을 설계하는 논리, 그리고 나무가 아닌 숲을 보는 안목을 가르쳐 주신 지도 교수님 **신성재 교수님**께 깊은 감사의 인사를 올립니다. 바쁘신 와중에도 제 학위에 많은 관심을 가져주시고 아낌없는 조언을 보내주신 **유지환 교수님**, **박상철 교수님**께도 깊은 감사의 인사를 올립니다.

실험실에서 오랜 시간 함께하며 서로 의지가 되어주고, 때로는 격려와 응원으로 버팀목이 되어준 TB Lab 식구들께도 특별한 감사 말씀드립니다. 항상 밝은 미소로 저를 아껴주시는 최홍희 선생님, 언제나 따뜻한 마음으로 하나라도 더 알려주시고 챙겨 주시는 김이한 박사님, 늘 환하게 인사해주시는 박지해 박사님, 어려운 것도 이해하기 쉽게 설명해주시는 김홍민 박사님 감사드립니다. 특히, 늘 든든한 큰오빠처럼 함께해주는 멋진 산이오빠, 항상 밝게 이름 불러주면서 반겨주던 은솔오빠, 푸근한 미소로 항상 으쌰으쌰 해주는 하규오빠, 선배이자 친구로 내가 정말 많이 믿고 의지했던 고마운 지윤이, 뭐 하나라도 더 알려주고 항상 챙겨주려고 하는 감사한 상원오빠, 비슷한 시기에 들어와 서로 의지를 많이 했던 속이 참 깊은 예린이, 항상 소소한 농담으로 웃게 만들어주는 경민이, 뭐든 척척 똑 부러지는 원석이, 언제나 천사 같은 마로오빠, 현지언니, 인곤오빠, 지은쌤, 혜수쌤 감사드리고, 새로 오신 정도헌 박사님과 유빈쌤까지 누구 하나 빠짐없이 모두의 존재가 참으로 소중하고 곁에서 항상 도와주시고 응원해주신 덕분에 학위를 잘 마칠 수 있었다고 생각합니다. 무엇보다 마지막까지 저를 믿고 이끌어주며 포기하지 않도록 함께해준 주미언니에게 깊은 감사의 마음을 전합니다. 또한, 항상 제 일상에 행복이 가득하길 진심으로 바라주시는 상철선생님, 다희언니, 예은언니에게도 진심으로 감사드립니다.

끝으로, 힘들고 지칠 때마다 늘 제 곁을 지켜주고 묵묵히 응원해준 친구들과 사랑하는 가족에게도 진심 어린 고마움을 전합니다. 지금껏 받은 많은 도움과 은혜를 앞으로의 삶 속에서 하나하나 되돌려 드릴 수 있는 사람이 되겠습니다.

TABLE OF CONTENTS

LIST OF FIGURES

Chapter I

Chapter II

LIST OF TABLES

ABSTRACT

Dissection of immunomodulatory mechanisms in chronic lung disease under various conditions

Chronic lung diseases such as tuberculosis (TB) and asthma involve chronic inflammation mediated by complex interactions between structural and immune cells. Alternative approaches to immune regulation may offer potential for disease amelioration by targeting multiple immune pathways. Developing immune regulatory approaches that can control chronic inflammation and minimize tissue injury is essential in managing lung diseases such as tuberculosis and asthma.

In this study, I examined immunoregulatory mechanism using different disease models. One focused on the role of NOX4, a member of the NADPH oxidase family, in controlling immune responses during *Mycobacterium tuberculosis* (Mtb) infection and asthma. The other of the study explored whether colchicine, known for its anti-inflammatory effects, could modulate adaptive immune mechanisms involved in asthma.

In a mouse model of TB, a diminished bacterial burden and reduced pulmonary inflammation were observed in the context of NOX4 deficiency. *Nox4*$^{-/-}$ mice exhibited increased infiltrated dendritic cells (DCs) and increased proportions of $CD4^+$ T cells secreting IFN-γ. Mechanistically, DCs from *Nox4*$^{-/-}$ mice showed augmented IL-12 expression, mediated by IRF1 activation through the AKT/GSK-3β pathway. This enhanced IL-12 response facilitated more effective Type 1 helper cell polarization and immune control of Mtb. Moreover, Bacillus Calmette-Guérin vaccination was more efficacious in *Nox4*$^{-/-}$ mice, indicating that NOX4 negatively regulates protective immunity under Mtb infection and potentially indicate a promising adjuvant target for TB vaccines.

In a separate model of asthma, NOX4 deficiency alleviated bronchial inflammation and mucus production but did not significantly affect Type 2 helper cell (Th2) cytokine levels

or eosinophil recruitment. In contrast, colchicine significantly suppressed the secretion of IL-4 and IL-13 from stimulated $CD4^+$ T cells and led to a significant reduction in eosinophil infiltration within both lung tissue and bronchoalveolar lavage fluid in a mouse model of conventional asthma. However, colchicine failed to reverse established histopathological changes, suggesting a dissociation between cytokine modulation and tissue remodeling. These results underscore the necessity of targeting both innate epithelial signaling and adaptive immunity for effective asthma control.

Taken together, this dual-chapter investigation illustrates that NOX4 regulates innate immune cell function and tissue inflammation across two distinct pulmonary disease contexts. Meanwhile, colchicine exerts selective effects on Th2-mediated cytokine responses without fully resolving structural pathology. These findings suggest that targeting oxidative stress or employing anti-inflammatory agents such as colchicine may represent a meaningful therapeutic approach for regulating inflammation in chronic lung diseases. In particular, modulating immune responses to alleviate inflammation may serve as an effective treatment option, with NOX4 emerging as promising immunoregulatory target in this context.

Key words: *Mycobacterium tuberculosis*, NADPH oxidase 4, dendritic cells, type 1 T helper cells, asthma, colchicine, eosinophils, type 2 T helper cells

Chapter I
NADPH Oxidase 4 deficiency enhances dendritic cell mediated IL-12 production and responses in *Mycobacterium tuberculosis* infection

1.Introduction

Tuberculosis (TB), caused by *Mycobacterium tuberculosis* (Mtb), remains one of the leading causes of global mortality.[1] Despite the Bacillus Calmette-Guérin (BCG) vaccine and over 20 anti-TB drugs, the TB burden remains high, with 10.8 million new cases reported in 2023, and a disrupted decline due to the COVID-19 pandemic.[1,2]

Reactive oxygen species (ROS) are crucial for the host defense against Mtb complex infections, with nicotinamide adenine dinucleotide phosphate oxidase (NOX) serving as a primary contributor to their generation.[3,4] Among the NOX isoforms, NOX4 plays a key role in immune regulation and fibrosis, including during infections caused by *Toxoplasma gondii*, *Listeria monocytogenes*, *Chlamydia trachomatis*, Influenza A virus, and *Staphylococcus aureus.*[5-9] It also contributes to pulmonary fibrosis, such as in idiopathic pulmonary fibrosis.[10] In Mtb infection, NOX4 is linked to TB fibrosis in mesothelial cells exposed to heat-killed Mtb.[11-13]

Innate immune cells such as macrophages and dendritic cells (DCs) serve as the first line of defense against Mtb and are essential for shaping the adaptive immune responses.[14] DCs, in particular, serve as essential antigen-presenting cells linking innate and adaptive immunity by recognizing Mtb through pattern recognition receptors.[15] This triggers cytokine secretion, including interleukin-12 (IL-12), tumor necrosis factor-α (TNF-α), and IL-10, and upregulation of surface molecules (MHC-I, MHC-II, CD 40, CD80, and CD86), enabling DC migration to lymph nodes to activate T cells, producing interferon (IFN)-γ, TNF-α and IL-17.[16-18] IL-12, a key driver of the Th1 response and a heterodimer of IL-12p35 and IL-12p40, promotes Mtb protection by enhancing the survival and function of

memory $CD4^+$ T cells.[19-21]

While NOX4's role in macrophage function, including polarization and proinflammatory cytokine production, is well-documented,[22,23] its impact on DCs, key orchestrators of T cell immunity, remains underexplored in the context of TB. Given the central role of DCs in shaping adaptive immunity, we hypothesized that NOX4 modulates DC function and downstream T cell responses during Mtb infection.

The current study reveals that NOX4 absence enhances DC infiltration and activation., increasing IL-12 secretion via the AKT-GSK3β-IRF1 axis. This promotes Th1 differentiation, reduces bacterial load, and mitigates inflammation, highlighting NOX4 as a potential target for boosting DC-mediated immunity in TB treatment.

2.Materials and methods

2.1. Ethics statement

All animal procedures were conducted in accordance with the regulations established by the Korean Food and Drug Administration. The study protocols received prior approval from the Institutional Animal Care and Use Committee (IACUC) of Yonsei University College of Medicine (Approval No. 2016-0178 and 2019-0174).

2.2. Mice

Male C57BL/6N wild-type (WT) mice, aged 6-7 weeks, were obtained from Japan SLC, Inc. in Shizuoka, Japan, while age-matched *Nox4*$^{-/-}$ mice were generously provided by Dr. Ji-Hwan Ryu at Yonsei University and Dr. Yun Soo Bae at Ewha Womans University in Seoul, South Korea. Briefly, *Nox4*$^{-/-}$ mice were originally generated via homologous recombination using a targeting construct based on genomic DNA from 129/SvJ embryonic stem cells. The resulting chimeras were subsequently backcrossed onto the C57BL/6N background, as previously described.[24,25] The mice were maintained under biosafety level-3 conditions with a regulated temperature of 24 ± 1°C, 50 ± 5% humidity, and a 12-h light and dark phases, with unrestricted supply of food and water. After a one-week acclimatization, all mice were healthy and monitored daily until the endpoint of the infection challenge.

2.3. Preparation of Mtb K strain

The Mtb K strain (Beijing lineage) was obtained from the Korean Institute of Tuberculosis in Osong, South Korea.26 The Mtb K strain was cultured as previously described.[26,27]

2.4. Bacterial load and lung inflammation post-Mtb infection

WT and *Nox4*$^{-/-}$ mice (n = 3-5 / naive group, n = 4 / infection group) were infected with

the Mtb K strain via aerosol using a Glas-Col aerosol device (Terre Haute, IN, USA). The infection was calibrated to deliver an initial dose of approximately 160 colony-forming units (CFUs) per mouse, as described in previous studies.[3,28,29] At two- and four-weeks post-infection, mice were euthanized for bacterial load and lung pathology analysis. Left lung lobes were homogenized, serially diluted, and cultured on 7H10 agar supplemented with 10% OADC and 0.5% amphotericin B (Sigma-Aldrich). Plates were incubated (37°C, 5% CO2) for 3-4 weeks to enumerate CFUs. Right superior lung lobes were fixed, paraffin-embedded, and sectioned (4-5 μm), and stained with hematoxylin and eosin (H&E) for inflammation assessment. Inflamed areas were measured using ImageJ (NIH, Bethesda, MD, USA) and expressed in mm^2.

2.5. Mtb infection challenge in female mice

Female WT and *Nox4*$^{-/-}$ mice (n = 4-5 per group) were infected via aerosol challenged with Mtb K strain (265 CFU/mouse). At four weeks post-infection, mice were sacrificed for bacterial load and lung pathology analysis. Lung preparation and histological analysis were conducted as described in the Materials and Methods section.

2.6. BCG vaccination challenge

Male WT and *Nox4*$^{-/-}$ mice (n = 4-6 per group) were subcutaneously vaccinated with BCG Pasteur 1173P2 (1 x 106 CFU/mouse), which was provided by Dr. Brosch at the Pasteur Institute (Paris, France) and cultured as described in the Materials and Methods section. Six weeks post-vaccination, mice were aerosol-challenged with Mtb K strain (310 CFU/mouse). Four weeks later, mice were euthanized for bacterial burden analysis, histopathology.

2.7. Lung cell preparation

Lung tissues were minced and incubated in Roswell Park Memorial Institute 1640 Medium (RPMI 1640; Biowest, Nuaillé, France), supplemented with 10% fetal bovine

serum (FBS; Biowest), 0.1% collagenase type II (Worthington-Biochem, Lakewood, NJ, USA), 1mM CaCl2, and 1mM MgCl2 at 37°C for 30 min. After erythrocyte lysis using ACK buffer (ThermoFisher Scientific, Waltham, MA, USA), the single cells were collected.

2.8. Immune profiling by flow cytometry in Mtb-infected mice

Lung cells (4×10^5 cells/well) were seeded, blocked with anti-CD16/32 antibody, and stained with LIVE/DEAD™ and surface marker antibodies (anti-CD45, anti-F4/80, anti-CD11b, anti-CD11c, anti-CD90.2, anti-MHC-II). For intracellular cytokine analysis, the cells were stimulated with either 5 μg/ml purified protein derivative (PPD) or 1 μg/ml early secreted antigenic target 6-kDa (ESAT-6) and GolgiPlug/GolgiStop (BD Bioscience, San Jose, CA, USA) for 12 h, and stained with surface markers (anti-CD90.2, anti-CD4, anti-CD8, and anti-CD44), and intracellular anti-IFN-γ and anti-TNF-α. After washing and fixation with IC Fixation buffer (Invitrogen, Waltham, Ma, USA), cells were analyzed using a CytoFLEX S Flow Cytometer (Beckman-Coulter, IN, CA, USA) and FlowJo™ software (Tree Star, Inc., Ashland, Oregon, USA). Table 1 contains detailed information on the antibodies.

2.9. Quantification of cytokines in Mtb-infected mice

After stimulating lung cells (4×10^5 cells/well) with either 5 μg/ml PPD or 1 μg/ml ESAT-6 for 12 h, cytokine levels (IFN-γ, TNF-α, IL-10) were quantified using ELISA kits (Invitrogen and BioLegend, San Diego, CA, USA), in accordance with the manufacturer′s procedures. Table 2 contains detailed information on the antibodies.

Table 1. List of fluorescently labeled antibodies utilized in this study

Antibodies	Dilution	Source	Identifier
Unconjugated rat monoclonal anti-mouse CD16/32 (clone 93)	1:400	BioLegend	Cat. No. 101320 RRID : AB_1574975
Surface staining			
LIVE/DEAD™ Fixable Aqua Dead Cell Stain Kit	1:1000	ThermoFisher Scientific	Cat. No. L34957
LIVE/DEAD™ Fixable Near-IR dead cell stain kit	1:1000	ThermoFisher Scientific	Cat.No. L34976
BD Horizon™ BV421 Rat Anti-Mouse CD45	1:400	BD Biosciences	Cat. No. 563890 RRID : AB_2651151
F4/80 Monoclonal Antibody (BM8), PE-Cyanine7, eBioscience™	1:400	ThermoFisher Scientific	Cat. No. 25-4801-82 RRID:AB_469653
PerCP/Cyanine5.5 anti-mouse/human CD11b Antibody	1:400	BioLegend	Cat. No. 101228 RRID:AB_893232
PE/Dazzle™ 594 anti-mouse CD11c Antibody	1:400	BioLegend	Cat. No. 117348 RRID:AB_2563655
Brilliant Violet 605™ anti-mouse CD90.2 (Thy1.2) Antibody	1:400	BioLegend	Cat. No. 140318 RRID:AB_2650924
MHC Class I (H-2Kd/H-2Dd) Monoclonal Antibody (34-1-2S), PE, eBioscience™	1:400	ThermoFisher Scientific	Cat. No. 12-5998-83 RRID:AB_466123
APC/Cyanine7 anti-mouse I-A/I-E Antibody	1:400	BioLegend	Cat. No. 107628 RRID:AB_2069377
Brilliant Violet 421™ anti-mouse I-A/I-E Antibody	1:400	BioLegend	Cat. No. 107632 RRID:AB_2650896
Brilliant Violet 421™ anti-mouse/human CD44 Antibody	1:400	BioLegend	Cat. No. 103040 RRID:AB_2616903
PerCP/Cyanine5.5 anti-mouse CD4 Antibody	1:400	BioLegend	Cat. No. 100540 RRID:AB_893326
Brilliant Violet 785™ anti-mouse CD8a Antibody	1:400	BioLegend	Cat. No. 100750 RRID:AB_25626

			10
FITC anti-mouse CD40 Antibody	1:400	BioLegend	Cat. No. 124608 RRID:AB_1134096
CD80 (B7-1) Monoclonal Antibody (16-10A1), APC, eBioscience™	1:400	ThermoFisher Scientific	Cat. No. 17-0801-82 RRID:AB_469417
BD Horizon™ V450 Rat anti-Mouse CD86	1:400	BD Biosciences	Cat. No. 560450 RRID:AB_1645280
Intracellular staining			
PE anti-mouse IFN-γ Antibody	1:200	BioLegend	Cat. No. 505808 RRID:AB_315402
BD Pharmingen™ APC Rat Anti-Mouse TNF-α	1:200	BD Biosciences	Cat. No. 554420 RRID:AB_398553

Table 2. The ELISA information used in this study

Antibodies (standard)	Top concentration (pg/ml)[1]	Sample dilution[2]	Source
IFN-γ	2000	1:8	Invitrogen
TNF-α	1000	1:4	Invitrogen
IL-12	2000	no dilution	Invitrogen
IL-10	2000	no dilution	BioLegend

[1] The highest concentration of each antibody standard was used to prepare a dilution series in the assay diluent, with the zero standard (0 pg/ml) consisting of the assay diluent alone.
[2] The samples were diluted using the assay diluent.

2.10. *In vitro* T cell proliferation and polarization via CD3/C28 stimulation

The plates were pre-coated with anti-CD3/CD28 monoclonal antibody (1 μg/ml) for 6 h at 37°C. Splenic $CD4^+$ T cells were isolated from both stains (WT and *Nox4*$^{-/-}$) naïve mice using magnetic-activated cell sorting (MACS, Miltenyi Biotec) system according to the manufacturers' protocol. The cells were labeled with 1 μM of CellTrace™ violet (ThermoFisher) and cultured in anti-CD3/CD28 pre-coated plates for three days. $CD4^+$ T cells were stained with fluorescent dye-conjugated antibodies (Table 1) and assessed for polarization by using a CytoFLEX S flow cytometer and FlowJo software. Supernatants from co-cultures were collected for IFN- γ measurement via ELISA, as previously described.

2.11. Preparation of bone marrow-derived macrophages

Bone marrow-derived macrophages (BMDMs) were generated from WT and *Nox4*$^{-/-}$ mice in DMEM containing 10% FBS, 1% P/S, and 10% L929 supernatant for 6 days, as previously described.

2.12. Intracellular anti-TB activities in BMDMs with IFN-γ stimulation

As previous studies described, BMDMs (3×10^5 cells/ml) were seeded overnight in a 48-well plate and infected with Mtb K in DMEM containing 5% FBS without P/S. Then, BMDMs were washed to remove extracellular bacteria at 4 h post-infection. Cells were treated with 15 ng/ml IFN- γ for 72 h, lysed with 0.05% Triton X-100, and lysates were plated on 7H10 agar to determine CFUs after three weeks.

2.13. Generation of BMDCs and Mtb infection

BMDCs were differentiated in RPMI 1640 containing 10% FBS, 1% penicillin/streptomycin (P/S; Sigma-Aldrich), 50 μM β-mercaptoethanol (ThermoFisher

Scientific), 0.1 mM non-essential amino acids (Sigma-Aldrich), 20 ng/ml recombinant mouse GM-CSF, and 5 ng/ml IL-4 (JW CreaGene Inc., Seongnam, South Korea) for 9 days, as outlined in previous protocols. 30-32 DC purity (>80%) was assessed using flow cytometry with LIVE/DEADTM, anti-CD11c, and anti-MHC-II antibodies. Antibody details are provided in Table 1. Following Mtb infection, supernatants were obtained, and the levels of cytokines (IL-12p70, TNF-α, IL-10) were analyzed using ELISA, as described above.

2.14. *In vitro* T cell proliferation and polarization by BMDC co-culture

Splenocytes from Mtb-infected WT and *Nox4*$^{-/-}$ mice were used to isolated CD4^{+} T cells via magnetic-activated cell sorting (MACS, Miltenyi Biotec, Bergisch Gladbach, Germany) system, in accordance with the manufacturer's procedures. Cells (2×10^5 cells/well) were labeled with 1μm of CellTrace™ violet (ThermoFisher Sientific) and co-cultured with Mtb-infected BMDCs (Multiplicity of infection [MOI] of 1, 4×10^4 cells/well) at a ratio of 1:5 between DCs and T cells for 3 days. T cell polarization was assessed by staining with fluorescent antibodies (Table 1) and characterized through flow cytometry and FlowJo software. Supernatants were collected for IFN-γ measurement via ELISA.

2.15. Analysis of cell surface molecule expression on DCs

On 9 days in culture, the BMDCs were harvested and washed once. Then BMDCs (1×10^6 cells/ml) were infected with Mtb K for 24 h. After incubation, the harvested cells were blocked Fc for 15 min at 4°C, followed by staining with PE/Dazzle-conjugated anti-CD11c (BioLegend), FITC-conjugated anti-CD40 (BioLegend), APC-conjugated anti-CD80 (ThermoFisher Scientific), V450-conjugated anti-CD86 (BD Bioscience), PE-conjugated anti-major histocompatibility complex (MHC) class I (ThermoFisher Scientific), APC-Cy7-conjugated anti-MHC class II (BioLegend) for 30 min at 4°C. The cells were analyzed with a CytoFLEX LS Flow cytometry (Beckman-Coulter) using FlowJo software.

2.16. Measurement of total ROS levels by flow cytometry

BMDCs from WT and *Nox4*$^{-/-}$ mice were harvested and surface marker stained with PE/Dazzle-conjugated anti-CD11c and APC-Cy7-conjugated anti-MHC class II for 30 min at 4°C. And then, cells were washed with pre-warmed DPBS and stained with 50mM H_2 DCFDA (1:1000) diluted with HBSS for 30 min at RT. After H_2DCFDA staining, cells were washed twice with pre-warmed DPBS. Finally, cells were resuspended in cold FACS buffer and immediately analyzed by flow cytometry.

2.17. Immunoblot analysis

BMDCs were harvested post-infection and lysed in RIPA buffer (Merck Millipore, Burlington, MA, USA) with protease and phosphate inhibitors. The supernatants were obtained, and equal protein concentrations were loaded onto sodium dodecyl sulfate-polyacrylamide gels and then transferred to PVDF membranes (Merk Millipore). Following blocking, the membranes were exposed to primary antibodies, and subsequently incubated with HRP-conjugated secondary antibodies. The anti-NOX4 antibody was kindly provided by Dr. Yun Soo Bae, Ewha University. And the antibodies used included anti-IRF1, anti-phospho-AKT1, anti-AKT1, anti-phospho-GSK3β, anti-GSK3β, and β-actin. Bands were detected and analyzed with ImageJ software. Table 3 contains detailed information on the antibodies.

Table 3. List of antibodies used in western blotting

Antibodies	Dilution	Source	Identifier
IRF-1 (D5E4) XP® Rabbit mAb	1:1000	Cell Signaling Technology	Cat. No. 8478 RRID:AB_10949108
p-AKT1 (phospho S473) antibody	1:1000	Abcam	Cat. No. 66138 RRID:AB_1140998
AKT antibody	1:1000	Cell Signaling Technology	Cat. No. 9272 RRID:AB_329827
p-GSK3β antibody (F-2)	1:1000	Santa Cruz Biotechnology	Cat. No. sc-373800 RRID:AB_10920410
GSK3β antibody (E-11)	1:1000	Santa Cruz Biotechnology	Cat. No. sc-377213 RRID:AB_2892800
NOX4 antibody	1:500	Provided by Dr. Yun Soo Bae (University of Ewha)	N/A
β-actin (13E5) Rabbit mAb	1:10000	Cell Signaling Technology	Cat. No. 4970 RRID:AB_2223172
Secondary Antibodies	**Dilution**	**Source**	**Identifier**
HRP-conjugated anti-rabbit IgG	1:3000	Millipore	Cat. No. 12-348 RRID : AB_390191
HRP-conjugated anti-mouse IgG	1:3000	Jackson ImmunoResearch Labs	Cat. No. 115-035-003 RRID : AB_10015289

2.18. Immunofluorescence staining

BMDCs were seeded at 1 × 10^6 cells/mL in Poly-L-Lysine 4-well culture slides for overnight. The next day, cells were infected with Mtb K at an MOI of 1 for 24 h. After infection, cells were washed with DPBS, fixed with 4% paraformaldehyde for 20 min at room temperature (RT), permeabilized with 0.1% Triton X-100 for 10 min, and blocked with 1% BSA in PBS-T (0.05% Tween-20) for 1 h. Cells were then incubated with anti-NOX4 overnight at 4°C, followed by an a 1 h incubation with Texas Red-conjugated goat anti-rabbit IgG (RRID: AB_2556776) at RT. Nuclei were counterstained with DAPI mounting solution (RRID: AB_10189288, Santa Cruz Biotechnology), and images were acquired using a Zeiss Thunder microscope.

2.19. RNA extraction and quantitative PCR

RNA extraction was performed utilizing TRIzol reagent (Thermo Fisher) with chloroform and isopropanol, then washed with 75% ethanol. The RNA was eluted in DEPC-treated water and quantified using a Thermo ScientificTM NanoDrop™ 2000 Spectrophotometer. Next, cDNA was synthesized from 1 μg of RNA using an RNA-to-cDNA EcoDryTM Premix (Oligo dT) (Takara Bio, Shiga, Japan), following the manufacturer's instructions. Gene expression was quantified through quantitative PCR (qPCR) using a StepOne Real-Time PCR system (Applied Biosystems, Thermo Fisher), with β-actin as the housekeeping gene, and relative expression was computed using the $2^{-\Delta\Delta Ct}$ method. The qPCR cycling conditions consisted of an initial 30-s denaturation at 95°C, followed by 45 cycles of 5 s at 95°C and 30 s at 62°C. Table 4 provides information on primer sequences. The data are from three independent experiments.

Table 4. List of qPCR primer sequences used in this study

Genes	Forward sequence	Reverse sequence
Il12a	5'-GTG CCT TGG TAG CAT CTA TGA-3'	5'-TGC CCT TGT CTA GAA TGA TCT G-3'
IL12b	5'-AGC ACG GCA GCA GAA TAA A-3'	5'-CTC CAC CTG TGA GTT CTT CAA A-3'
Ngatc4	5'-GCT TCG GAG CAG GAG AAA G-3'	5'-GGC CAA TGA TCT CAC TCA CTT-3'
Foxa2	5'-AAA TGG ACC TCA AGG CCT AC-3'	5'-CCC GCT TTG TTC GTG ACT-3'
Irf1	5'-GGA CAT TGG GAT AGG CAT ACA A-3'	5'-CAC AAG GAA TGG CCT GAA TAG A-3'
Jun	5'-AAA CTC CGA GCT GGC ATC-3'	5'-GAG TTG GCA CCC ACT GTT A-3'
β-actin	5'-CCG TAA AGA CCT CTA TGC CAA-3'	5'-AGG AGC CAG AGC AGT AAT CT-3'

2.20. IL-12 neutralization in BMDCs and BMDC-T cell co-culture assays

WT and *Nox4*$^{-/-}$ BMDCs (1 × 10^6 cells/ml) were plated and subsequently infected with Mtb K at a MOI of 1. To neutralize the biological effects of IL-12, 25 μg/ml of anti-mouse IL-12 antibody (Bio X cell, Lebanon, NH, USA) was added 24 h post-infection. The cells were incubated for 1 h at 37°C before initiating co-culture. Splenic $CD4^+$ T cells (1 × 10^5 cells/well), isolated from Mtb-infected WT mice using the MACS system, were co-cultured with IL-12-neutralized, Mtb-infected BMDCs (2 × 10^4 cells/well) at a DC to T cell ratio of 1:5 for 3 days. Following co-culture, supernatants were collected, and the levels of cytokines (IL-12p70 and IFN-γ) were quantified by ELISA, as described above.

2.21. RT^2 profiler PCR array

The relative mRNA expressions in WT and *Nox4*$^{-/-}$ BMDC (1 × 10^6 cells/ml) after 4 h Mtb infection was analyzed using an RT^2 ProfilerTM PCR array (Mouse transcription factors, Qiagen, HD, Germany), in accordance with the manufacturer's procedures. The data were analyzed via the RT^2 Profiler PCR Array Data Analysis website (https://dataanalysis2.qiagen.com/pcr), and mRNA changes were calculated with the ΔΔCt method. The Retrieval of Interacting Genes/Proteins (STRING) database was used to explore protein-protein interactions, which were then visualized using Cytoscape (version 3.10.1; https://cytoscape.org/).

2.22. Compound

SB216763, a GSK3β inhibitor (Sigma-Aldrich, Cat#S3442), was used to pretreat BMDCs at concentrations of 0.1 and 10 μM for 30 minutes before Mtb infection.

2.23. Statistical analysis

An unpaired *t-test* was used to assess statistical significance (GraphPad Prism version 9.00, La Jolla, CA, USA, www.graphpad.com). Data are presented as mean values with

standard deviation (S.D.). Significance levels were marked as *$p < .05$, **$p < .01$, ***$p < .001$ and ****$p < .0001$.

3.Results

3.1. NOX4 deficiency alleviated the bacterial burden and lung pathology in Mtb-infected mice

To explore the involvement of NOX4 in the development of TB, we utilized an infection model involving WT and *Nox4*$^{-/-}$ mice aerosol-infected with Mtb **(Figure. 1A)**. Mice were sacrificed at two and four weeks after infection to evaluate CFUs and histopathological changes. Between two- and four-weeks post-infection, Mtb exhibited significant growth in WT mice, whereas no detectable growth was observed in *Nox4*$^{-/-}$ mice **(Figure. 1B)**. Consistently, at four weeks post-infection, *Nox4*$^{-/-}$ mice demonstrated a notable reduction in bacterial load relative to WT mice **(Figure. 1C)**. Histopathological analysis further confirmed a reduction in pulmonary inflammation in Mtb-infected *Nox4*$^{-/-}$ mice, consistent with the observed differences in bacterial load **(Figure. 1D)**. Additionally, a comparable pattern was observed in the female mice group and BCG-vaccinated group **(Figure. 2)**. These results indicate that the absence of NOX4 could contribute to regulating mycobacterial proliferation and lung inflammation.

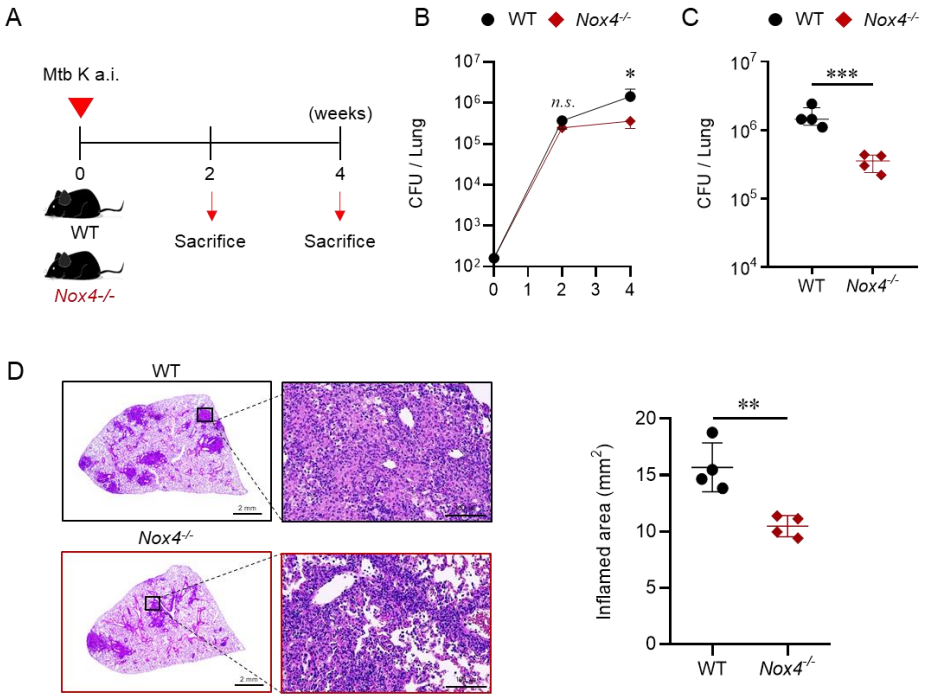

Figure 1. Controlled bacterial burden and improved pathology in the lungs of *Nox4*$^{-/-}$ mice with Mtb infection. (A) Scheme of *in vivo* Mtb infection experiment. Mice (WT and *Nox4*$^{-/-}$) were infected with Mtb K and analyzed at two and four weeks after infection. **(B)** Bacterial burden in the lungs was assessed by enumerating CFUs at two- and four-weeks post-infection and presented as the kinetics. **(C)** The bacterial CFUs in the lungs of Mtb-infected mice were analyzed by calculating the number of colonies at four weeks post-infection and presented as scatter dot plots. **(D)** Inflamed areas of the lungs were analyzed by H&E staining, and inflammation in the lungs of Mtb-infected mice were quantified at four weeks post-infection (10x: scale bar = 2.0 mm; 200x: scale bar = 100 μm) and presented as scatter dot plots. Data are shown as means ± S.D. (n = 4 mice/group). Statistical analysis was conducted by unpaired *t-test*. $^{**}p < .01$ and $^{****}p < .0001$.

Abbreviation: WT, C57BL/6N wild-type mice; *Nox4*$^{-/-}$, NOX4-deficient mice; Mtb, *Mycobacterium tuberculosis*; CFUs, Colony forming units.

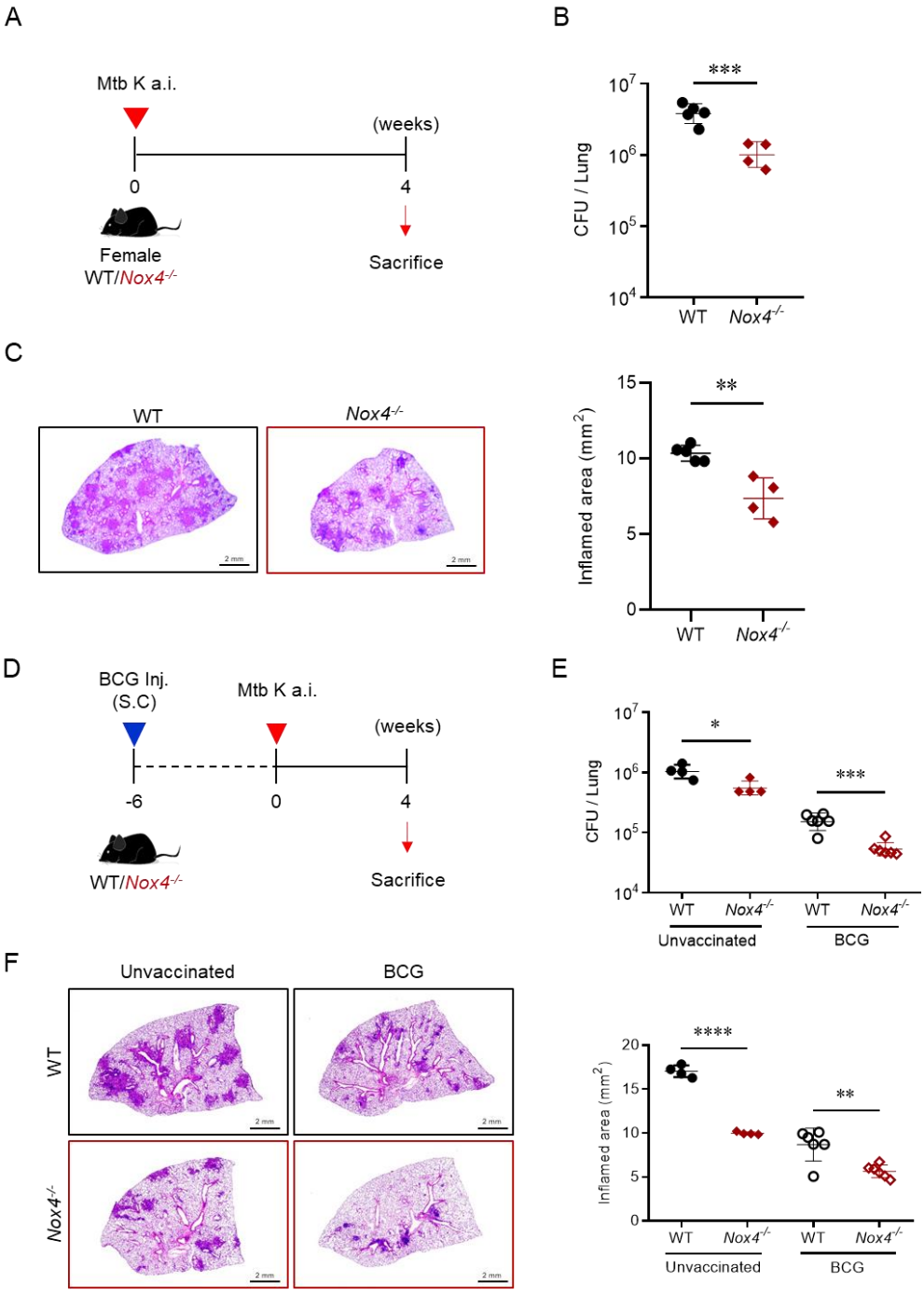

Figure 2. Improved Mtb control across infection settings in NOX4-deficient mice. (A) Scheme of the *in vivo* Mtb infection experiment using female WT and *Nox4*$^{-/-}$ mice. Mice were infected with Mtb K strain and analyzed four weeks post-infection. **(B)** Bacterial CFUs in the lungs were quantified by colony counting at four weeks post-infection. **(C)** Lung inflammation was assessed by H&E staining, with quantification of inflamed areas at four weeks post-infection (10x: scale bar = 2.0 mm) and presented as scatter dot plots. **(D)** Scheme of BCG vaccination and Mtb infection in mice *in vivo* experiment. Mice (WT and *Nox4*$^{-/-}$) were immunized with BCG six weeks before Mtb K infection and analyzed at four weeks post infection. **(E)** The bacterial CFUs in the lungs of unvaccinated and BCG vaccinated groups were analyzed by counting the number of colonies at four weeks post-infection. **(F)** Inflamed areas of the lungs were analyzed by H&E staining, and inflammation in the lungs of Mtb-infected mice were quantified at four weeks post-infection (10x: scale bar = 2.0 mm) and presented as scatter dot plots. Data are shown as means ± S.D. (n = 4-6 mice/group). Statistical analysis was conducted by unpaired *t-test*. *$p < .05$, **$p < .01$, ***$p < .001$ and ****$p < .0001$.

Abbreviation: WT, C57BL/6N wild-type mice; *Nox4*$^{-/-}$, NOX4-deficient mice; BCG, Bacillus Calmette-Guérin; Mtb, *Mycobacterium tuberculosis*; CFUs, Colony forming units.

3.2. NOX4 deficiency increased Th1 response in the lungs in Mtb-infected mice

Given that immune activation typically triggers a pro-inflammatory response in the lungs 2-3 weeks post-infection,[33,34] and that differences in bacterial burdens appear at 4 weeks in Figure. 1, we next analyzed immune cell profiles using flow cytometry at four weeks post-infection **(Figure. 3A)**. Notably, the lungs of *Nox4*$^{-/-}$ mice exhibited a marked increase in the CD45^{+} immune cell populations, especially DCs and T cells, following Mtb infection **(Figure. 3B)**. However, there were no notable differences in the alveolar and interstitial macrophage counts between Mtb-infected WT and *Nox4*$^{-/-}$ mice **(Figure. 3B)**. Based on the considerable increase in T cell populations in Mtb-infected *Nox4*$^{-/-}$ mice, we next explored whether NOX4 deficiency influences T cell responses after stimulation with 5 μg/ml PPD and 1 μg/ml ESAT-6, respectively, as outlined in the gating strategy of flow cytometry **(Figure. 4A)**. *Ex vivo* stimulation of lung cells with PPD and ESAT-6 revealed similar percentages of CD4^{+}CD44^{+} T cells in *Nox4*$^{-/-}$ and WT mice, but PPD and ESAT-6-specific CD4^{+}CD44^{+} T cells producing IFN-γ^{+} and TNF-α^{+} were significantly more abundant in *Nox4*$^{-/-}$ mice compared to WT mice **(Figure. 4B)**. In contrast, CD8^{+}CD44^{+} T cells producing IFN-γ^{+} after PPD and ESAT-6 stimulation showed no significant differences between *Nox4*$^{-/-}$ and WT mice **(Figure. 4C)**. Furthermore, we examined cytokine production in lung cells from Mtb-infected *Nox4*$^{-/-}$ and WT mice after *ex vivo* PPD and ESAT-6 stimulation. Only IFN-γ production was significantly higher in *Nox4*$^{-/-}$ mice **(Figure .4D)**. Collectively, these results highlight NOX4 as an essential regulator of IFN-γ production in the immune response to Mtb infection.

A

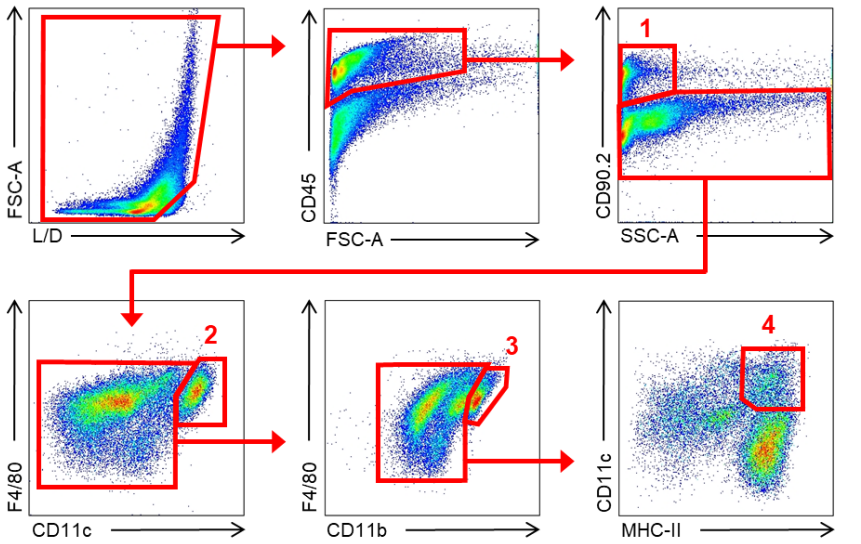

1. T cell
2. Alveolar Macrophage
3. Interstitial Macrophage
4. DC

B

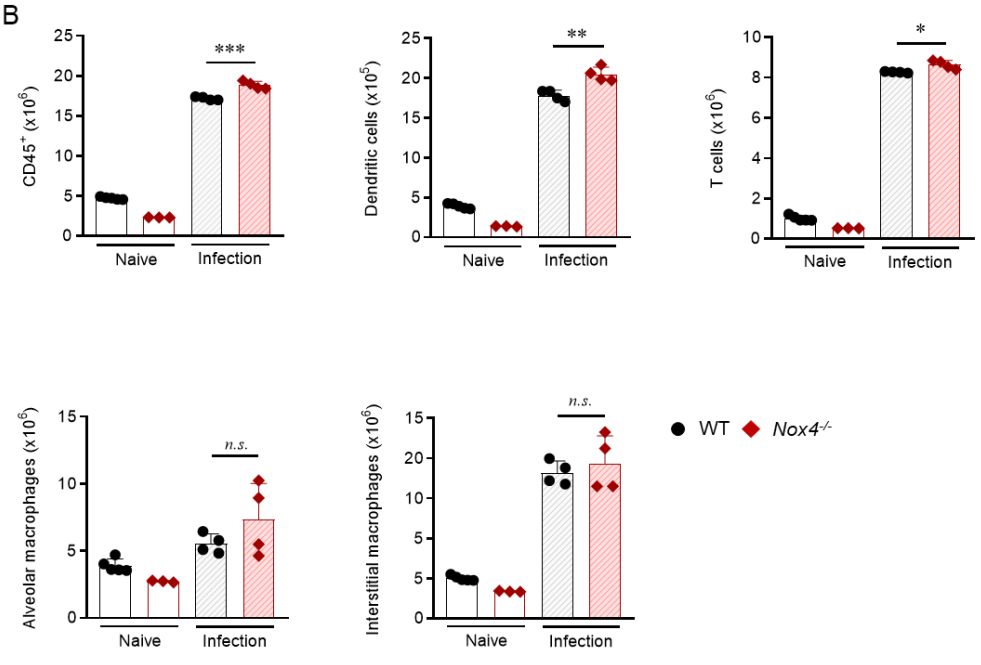

Figure 3. Characterization of immune cell populations in the lungs of Mtb infected mice by flow cytometry. (A) The gating strategy for T cells ($CD45^+CD90.2^+$), alveolar macrophages ($CD45^+CD90.2^-F4/80^+CD11c^+$), interstitial macrophages ($CD45^+CD90.2^-CD11c^-F4/80^+CD11b^+$), DC ($CD45^+CD90.2^-F4/80^-CD11b^-CD11c^+MHCII^+$) in the lungs of Mtb-infected mice at four weeks post infection. **(B)** The number of infiltrated immune cells, DC, T cells, alveolar and interstitial macrophages in the lungs four weeks post-infection was analyzed by flow cytometry. Data are shown as in bar graphs with dot plots. Data are shown as means ± S.D. (n = 3-5 mice/naive group, n = 4 mice/ infection group). Statistical analysis was conducted by unpaired *t-test*. *n.s.*: not significant. Abbreviation: DC, Dendritic cells.

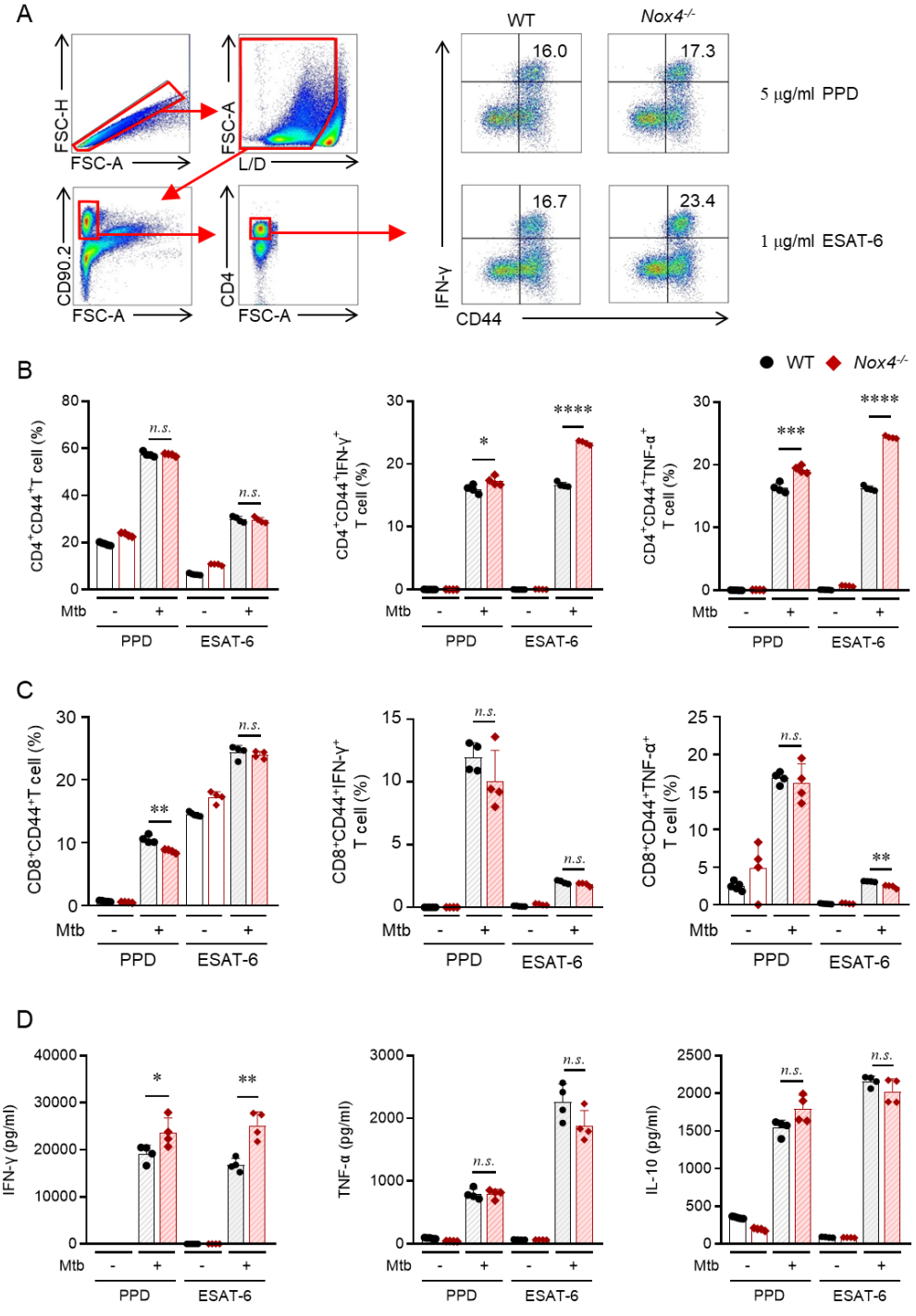

Figure 4. Increased Mtb-specific T cell responses in *Nox4*$^{-/-}$ mice. (A) Flow cytometry gating strategy was used to identify IFN-γ^+CD4$^+$CD44$^+$ T cells in the lungs at four weeks post-infection. The dot plot shows the frequency of IFN-γ^+CD4$^+$CD44$^+$ T cells after *ex vivo* stimulation with 5 μg/ml PPD and 1 μg/ml ESAT-6 in the lungs at four weeks post-infection. **(B)** The proportions of IFN-γ^+CD44$^+$CD4$^+$ T cells and TNF-α^+CD44$^+$CD4$^+$ T cells were analyzed by flow cytometry and illustrated as the bar graphs with dot plots. **(C)** The proportions of IFN-γ^+CD44$^+$CD8$^+$ T cells and TNF-α^+CD44$^+$CD8$^+$ T cells were analyzed by flow cytometry and illustrated as the bar graphs with dot plots. **(D)** Secreted levels of IFN-γ, TNF-α and IL-10 in suspended lung single cells after *ex vivo* stimulation with 5 μg/ml PPD and 1 μg/ml ESAT-6 were determined by ELISA and represented as bar graph accompanied by dot plots. Data are shown as means ± S.D. (n = 3-5 mice/naive group, n = 4 mice/infection group). Statistical analysis was conducted by unpaired *t-test*. *$p < .05$, **$p < .01$, ***$p < .001$, and *n.s.:* not significant.

Abbreviation: DC, Dendritic cells; PPD, Purified protein derivative; ESAT-6, early secreted antigenic target 6-kDa.

3.3. NOX4 deficiency enhanced IFN-γ production in T cells interacting with Mtb-infected DCs

To investigate the role of NOX4 in Th1 immune response, we assessed $CD4^+$ T cell proliferation and IFN-γ production after anti-CD3/CD28 stimulation **(Figure. 5A)**. T cell proliferation and IFN-γ production were similar between WT and *Nox4*$^{-/-}$ T cells, indicating that NOX4 does not affect the intrinsic function of T cells **(Figure. 5B–D)**. In addition, exogenous IFN-γ stimulation did not significantly alter the ability of BM-derived macrophages to control Mtb growth **(Figure. 5E)**. Then, we co-cultured splenic $CD4^+$ T cells from Mtb-infected WT mice with Mtb-infected BMDCs (5:1 ratio) for 3 days **(Figure. 6A)**. The expression of MHC-I, MHC-II, and co-stimulatory molecules on BMDCs was comparable in both groups **(Figure. 7)**, and T cell proliferation remained unchanged **(Figure. 6B)**. Furthermore, NOX4 deficiency did not alter total ROS levels in BMDCs following Mtb infection **(Figure. 8)**. However, a marked increase in IFN-γ production was observed in T cells co-cultured with *Nox4*$^{-/-}$ BMDCs, indicating enhanced T cell activation mediated by these BMDCs **(Figure. 6C)**. These results underscore that activated *Nox4*$^{-/-}$ BMDCs promote Th1 polarization and IFN-γ production.

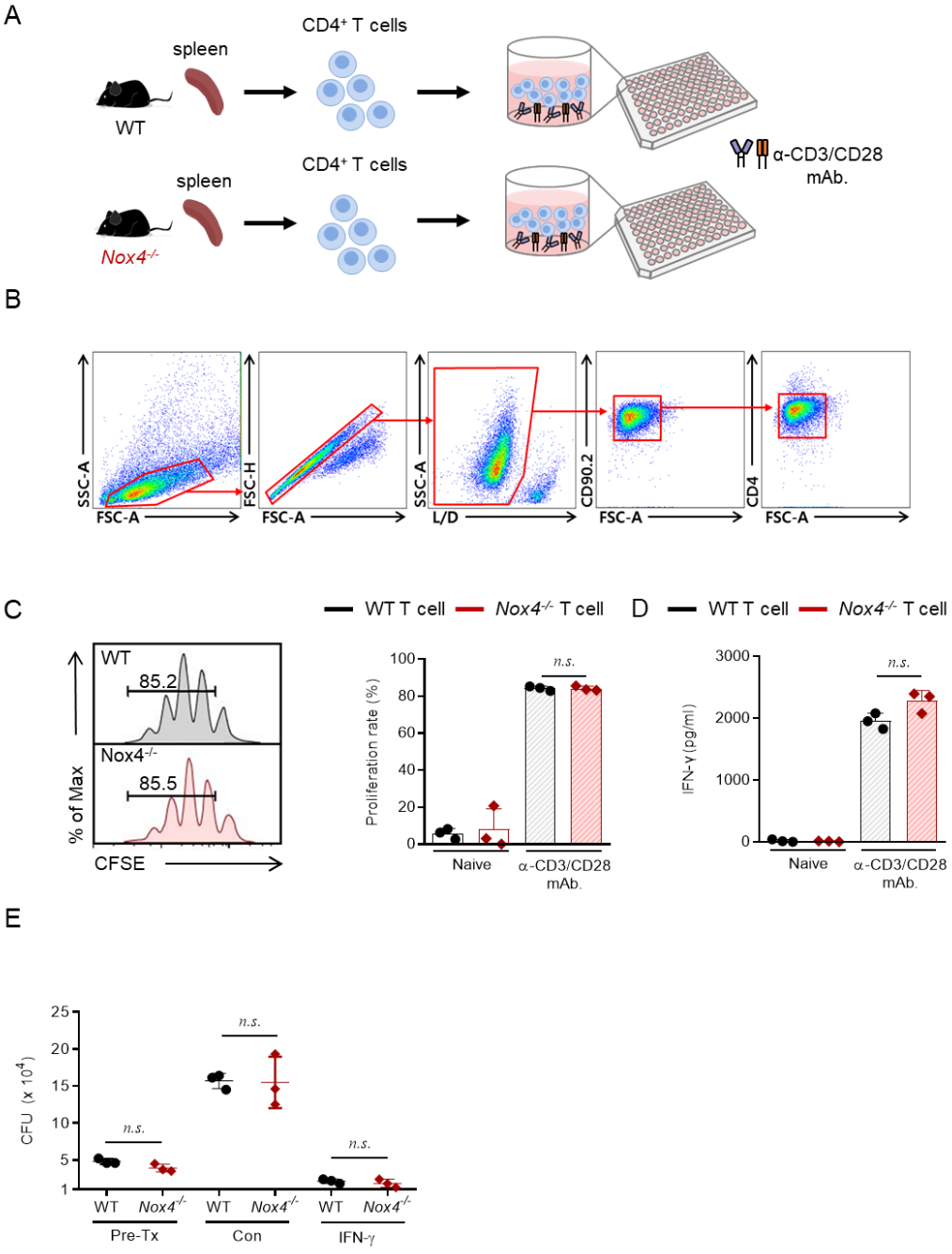

Figure 5. Investigation of intrinsic T cell response to CD3/CD28 monoclonal antibodies stimulation. (A) Scheme of $CD4^+$ T cell stimulation with α-CD3/CD28 mAb. Isolated naïve splenic $CD4^+$ T cells were cultured in α-CD3/CD28 mAb pre-coated plate for 6 h. **(B)** Gating strategy for isolated splenic $CD4^+$ T cells from naive WT and *Nox4*$^{-/-}$ mice using $CD4^+$ microbeads with MACS system. **(C)** Proliferation rate in $CD4^+$ T cells stimulated with α-CD3/CD28 mAb was analyzed by flow cytometry. The representative proliferation rate was shown by histogram and displayed by the bar graphs with dots. **(D)** Secreted IFN-γ protein levels in CD3/CD28-stimulated $CD4^+$ T cells supernatant was measured by ELSIA. **(E)** Bacterial burden in Mtb K-infected BMDMs was assessed by CFU enumeration following 15 ng/ml IFN-γ stimulation. The experiment was independently repeated at least three times, with representative results shown. Each dot represents the mean value ± S.D. of triplicate wells (averaged from four spots per well). Data are shown as means ± S.D. Statistical analysis was conducted by unpaired *t-test*. *n.s.*: not significant.

Abbreviation: α-CD3/CD28 mAb., CD3/CD28 monoclonal antibodies; MACS, Magnetic-activated cell sorting; Pre-Tx, 4 h post-infection (before IFN-γ stimulation); Con, infection control.

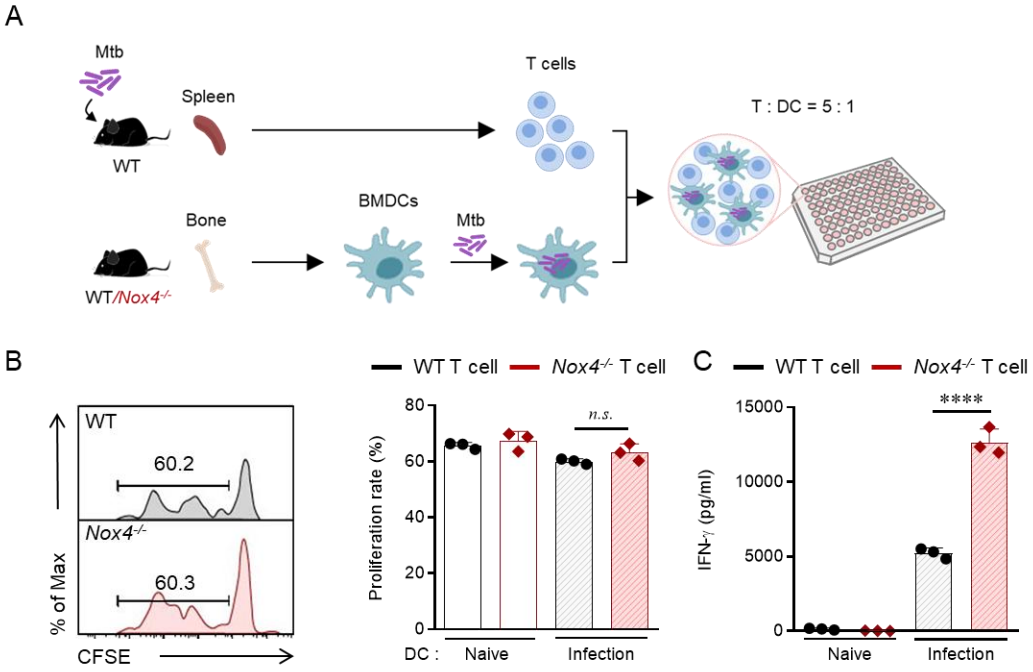

Figure 6. Enhanced IFN-γ production in T cells by co-culturing *Nox4*$^{-/-}$ BMDCs.

(A) Scheme of DC-T cell co-culture. Splenic CD4^{+} T cells, isolated from Mtb infected WT mice, and BMDCs from mice (WT and *Nox4*$^{-/-}$) were infected with Mtb K for 24 h and then co-cultured for three days. **(B)** Proliferation rate in BMDC-WT CD4^{+} T cell co-culture were assessed using flow cytometry. The representative proliferation rate was shown by histogram and presented as bar graphs with dot plots. **(C)** IFN-γ production levels in BMDC-WT CD4^{+} T cell co-culture supernatant was determined by ELISA and shown in bar graphs with dot plots. The experiments were independently repeated at least three times, and the results from a representative experiment are presented. Data are shown as means ± S.D. Statistical analysis was conducted by unpaired *t-test*. ****$p < .0001$, and *n.s.*: not significant.

Abbreviation: BMDCs, Bone marrow-derived dendritic cells.

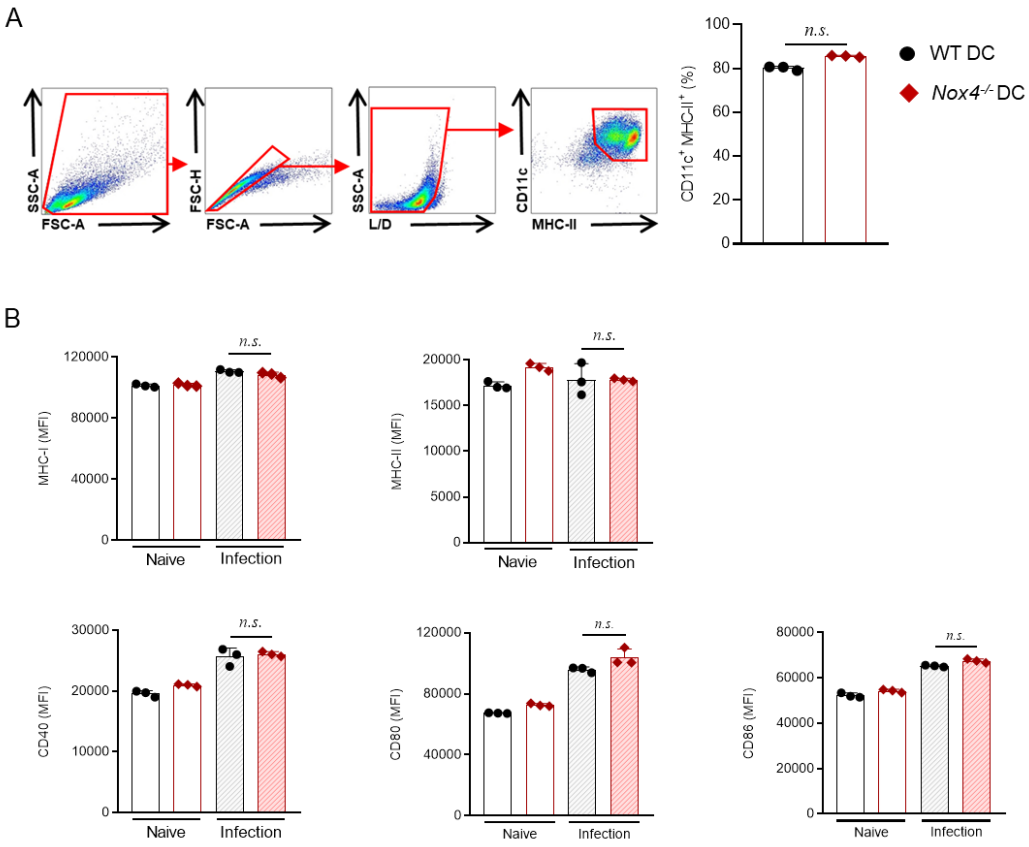

Figure 7. Assessment of BMDCs purity and maturation after Mtb-infected BMDCs by flow cytometry. (A) Gating strategy for BMDCs purity at 9 days post-differentiation is shown as pseudocolor dot plots, with the percentage of $MHCII^{+}CD11c^{+}$ cells displayed as the bar graphs with dot plots. **(B)** BMDC Maturation 24 h after Mtb infection was evaluated by surface marker expression, represented as bar graphs with dot plots. The experiments were independently repeated at least three times, and the results from a representative experiment are presented. Data are shown as means ± S.D. Statistical analysis was conducted by unpaired *t-test*. *n.s.*: not significant.

Abbreviation: BMDCs, Bone marrow-derived dendritic cells.

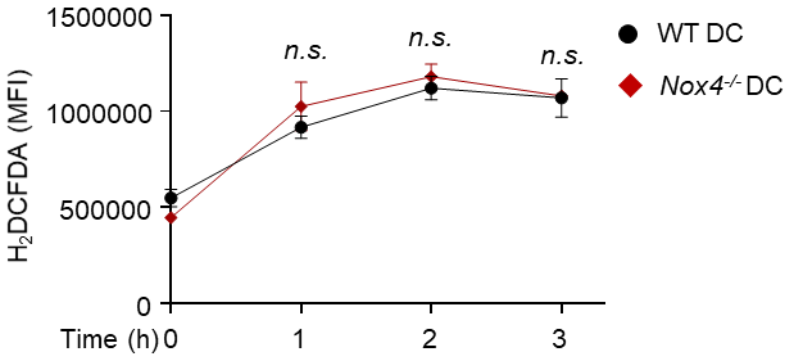

Figure 8. Measurement of Total ROS in WT and *Nox4*$^{-/-}$ BMDCs. BMDCs from (WT and *Nox4*$^{-/-}$) mice were infected with Mtb for a time course of 1, 2, and 3 h, followed by intracellular H_2DCFDA detection in BMDCs using flow cytometry. Data are shown as means ± S.D. Statistical analysis was conducted by unpaired *t-test*. *n.s.*: not significant. Abbreviation: hpi, hours post-infection.

3.4. NOX4 deficiency increased IL-12 production in Mtb-infected DCs

After confirming NOX4 expression in WT BMDCs and its absence in *Nox4*$^{-/-}$ BMDCs **(Figure. 9)**, we next analyzed cytokine profiles of BMDCs from WT and *Nox4*$^{-/-}$ mice following Mtb infection. *Nox4*$^{-/-}$ BMDCs secreted higher IL-12p70 levels in an MOI-dependent manner, with no changes in TNF-α and reduced IL-10 compared to WT BMDCs **(Figure. 10A)**. IL-12p70 levels in *Nox4*$^{-/-}$ BMDCs increased significantly at 4 h post-infection, peaking at 12 h, compared to WT BMDCs **(Figure. 10B)**. Since IL-12p70 consists of two subunits, we examined *Il12a* (encoding IL-12p35) and *Il12b* (encoding IL-12p40) mRNA levels, which were higher in *Nox4*$^{-/-}$ BMDCs, peaking at 4 h post-infection **(Figure. 10C)**. To determine the functional significance of IL-12p70 upregulation, neutralizing antibodies were applied during the BMDCs-T cell co-culture **(Figure. 11A)**. Effective blockade was confirmed by a reduction in IL-12p70 levels measured by ELISA in BMDCs treated with 25 μg/ml IL-12 neutralizing antibody **(Figure. 11B)**. Although IL-12 neutralization my not completely suppress IFN-γ secretion, it significantly reduced IFN-γ levels **(Figure.11C)**, thereby conforming that the elevated IL-12p70 in *Nox4*$^{-/-}$ BMDCs plays an essential role in driving Th1 activation **(Figure. 11C)**. These findings indicate that NOX4 regulates Mtb-specific IL-12p70 expression in BMDCs, promoting Th1 activation.

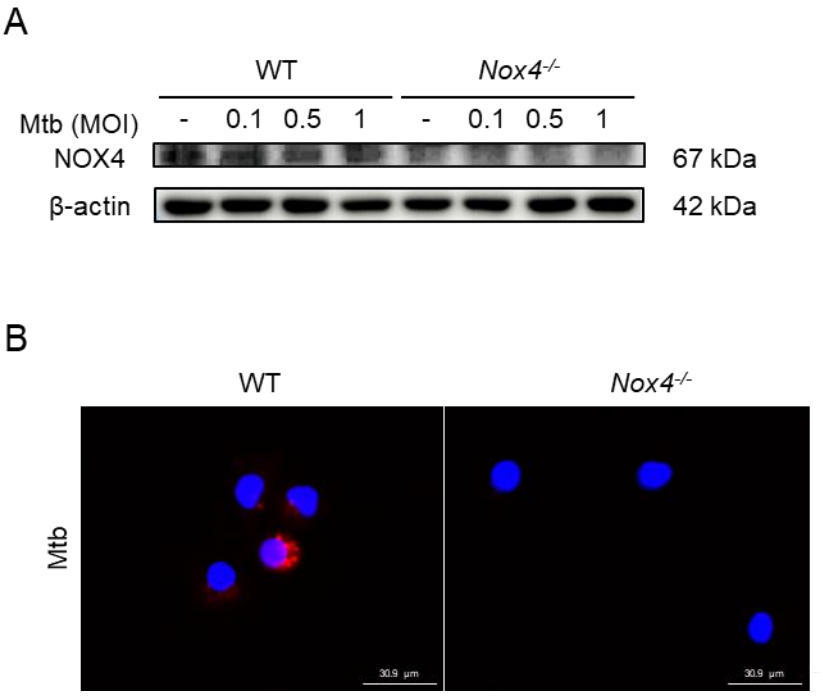

Figure 9. Detection of increased NOX4 expression in BMDCs following Mtb infection by immunoblot assay. (A) Representative immunoblots of NOX4 and β-actin in BMDCs from WT and *Nox4*$^{-/-}$ mice infected with Mtb at indicated MOIs for 8 h are displayed. **(B)** BMDMs were infected with Mtb at an MOI 1 for 24 h. Cells were stained with NOX4 and DAPI and visualized using thunder microscopy (scale bar = 30.9 μm).

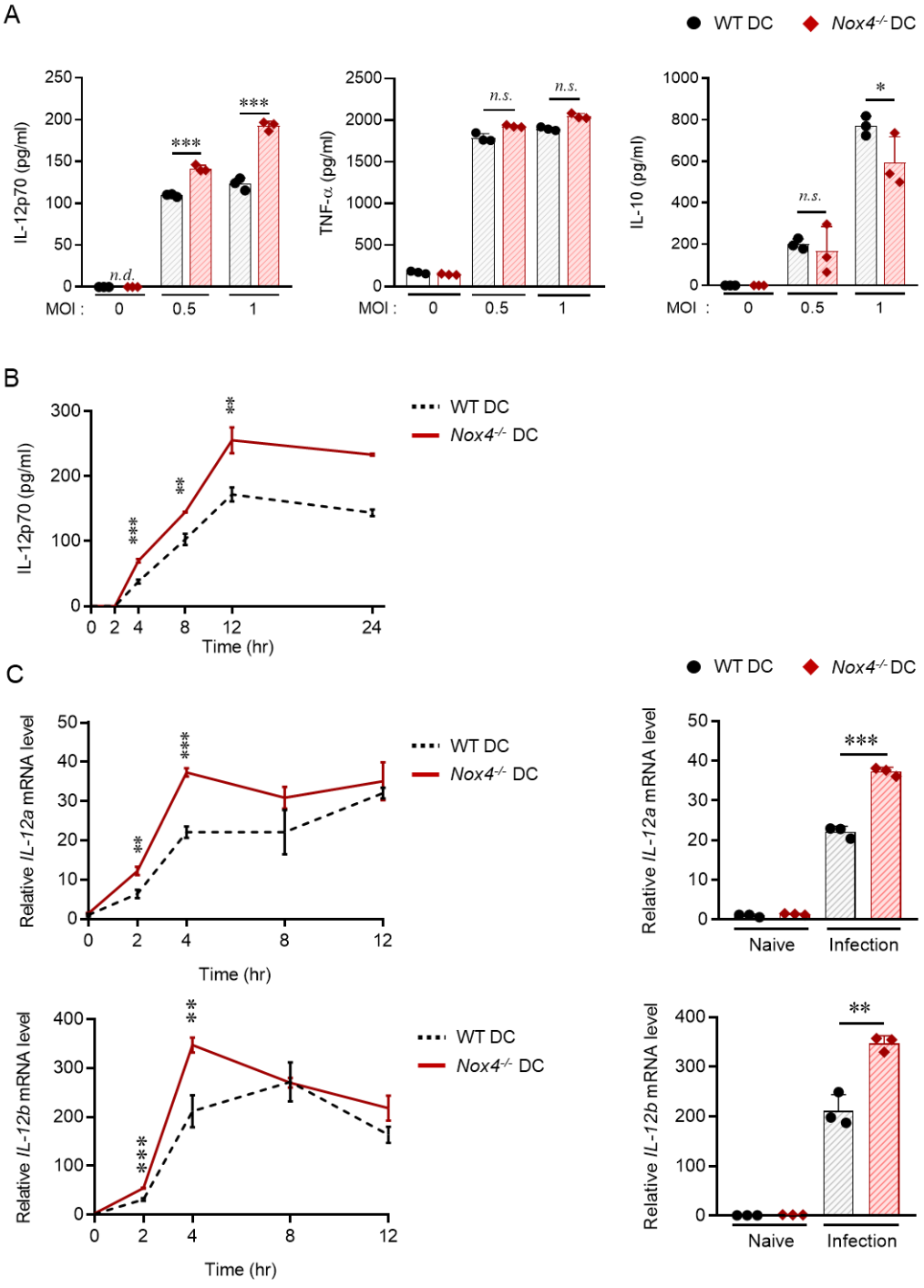

Figure 10. Increased IL-12p70 production in Mtb-infected *Nox4*$^{-/-}$ BMDCs. (A) MOI-dependent response of cytokine production in Mtb-infected BMDCs at 24 h. Secreted IL-12p70, TNF-α and IL-10 were determined by ELISA and displayed in bar graphs with dot plots. **(B)** Time-dependent response of IL-12p70 in Mtb-infected BMDCs was determined by ELISA and visualized through line graphs. **(C)** *Il12a* and *Il12b* mRNA expression in Mtb-infected BMDCs were measured by qPCR and illustrated with bar graphs with dot plots. *β-actin* was used as the normalization control. The experiments were independently repeated at least three times, and the results from a representative experiment are presented. Data are shown as means ± S.D. Statistical analysis was conducted by unpaired *t-test*. **p* < .05, ***p* < .01, ****p* < .001 and *n.s.:* not significant.
Abbreviation: MOI, Multiplicity of infection

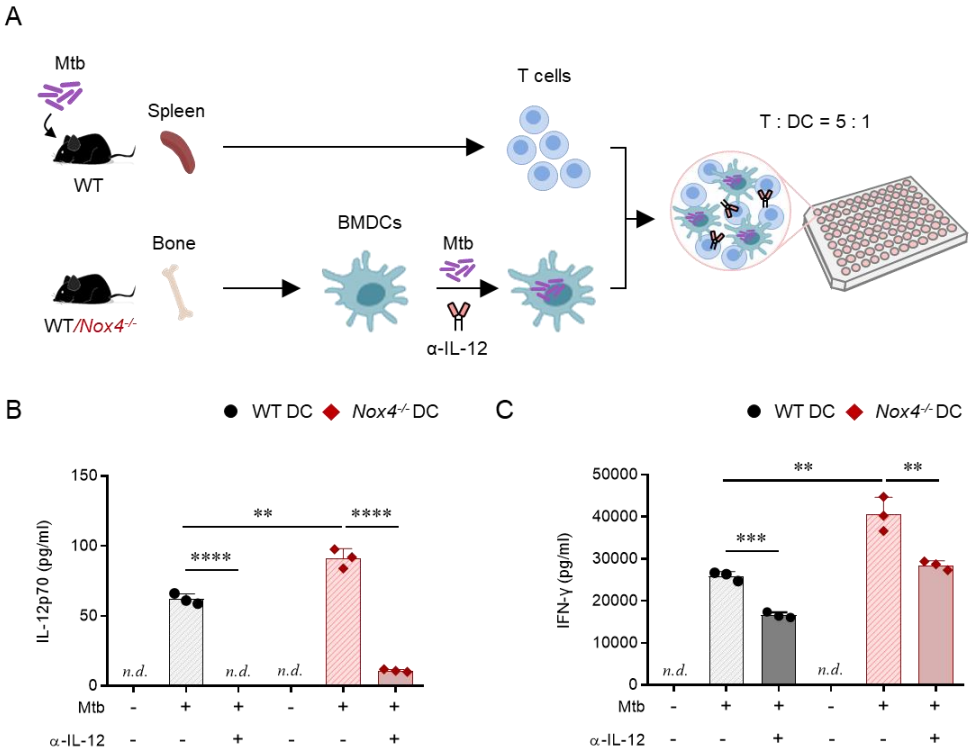

Figure 11. Reduced IFN-γ production upon IL-12 neutralization in BMDC-T cell co-culture. (A) Scheme of BMDC-T cell co-culture with IL-12 neutralization. BMDCs from mice (WT and *Nox4*$^{-/-}$) were infected with Mtb K for 24 h, followed by treatment with anti-mouse IL-12 antibody (25 μg/ml). After 1 h of neutralization, Splenic CD4^{+} T cells isolated from Mtb infected WT mice were co-cultured with BMDCs for three days. **(B)** IL-12p70 levels in the supernatants of Mtb-infected BMDCs was measured by ELISA at 24 h post-infection, following IL-12 neutralization 1 h prior to infection, and are shown as bar graphs with dot plots. **(C)** IFN-γ level in BMDC-WT CD4^{+} T cell co-culture supernatant was determined by ELISA after 3 days and shown in bar graphs with dot plots. The experiments were independently repeated at least three times, and the results from a representative experiment are presented. Data are shown as means ± S.D. Statistical analysis was conducted by unpaired *t-test*. **$p < .01$, ***$p < .001$ and ****$p < .0001$.

3.5. NOX4 regulated IL-12 production via AKT1-GSK-3β-IRF1 axis in Mtb-infected DCs

To identify transcription factors regulating IL-12p70 secretion under NOX4 deficiency, we performed an RT^2 profiler PCR array at 4 h post-infection. Among 24 differentially expressed genes in *Nox4*$^{-/-}$ BMDCs compared to WT BMDCs, 22 were upregulated and 2 were downregulated **(Figure. 12A and Table 5)**. The top two genes, *Nfatc4* and *Foxa2*, were validated by qPCR for the array **(Figure. 12B)**. Using STRING, a tool for predicting protein-protein associations, we identified *Irf1* and *Jun* as direct interactors with *Il12a* and *Il12b* **(Figure. 12C)**. Given the pivotal role of IRF1 in IL-12p70 production, we examined its activation in Mtb-infected *Nox4*$^{-/-}$ BMDCs. The mRNA expression levels of *Irf1* and *Jun* were validated. While *Irf1* was significantly upregulated in *Nox4*$^{-/-}$ BMDCs, *Jun* expression remained unchanged **(Figure. 12D)**. Moreover, IRF1 protein expression level was significantly elevated at 4, 8, and 12 h post-infection compared to WT BMDCs **(Figure. 13A, B)**. Since IRF1 activation is influenced by GSK-3β dephosphorylation and suppressed by AKT1 via GSK-3β phosphorylation,[35,36] we investigated AKT1 and GSK-3β regulation by NOX4. In *Nox4*$^{-/-}$ BMDCs, p-AKT1 and p-GSK-3β expression levels were significantly reduced at 30- and 60-min post-infection compared to WT BMDCs **(Figure. 13C-E)**. To determine whether GSK-3β regulates IRF1 activation, we assessed IRF1 expression level following treatment with 0.1 or 10 μM SB216763, a selective GSK-3 inhibitor **(Figure. 13F, G)**. Notably, 10 μM SB216763 significantly reduced IRF1 expression in Mtb-infected *Nox4*$^{-/-}$ BMDCs. Consequently, IL-12p70 secretion was also significantly decreased under the same conditions, whereas no significant effects were observed in WT BMDCs **(Figure. 13H)**. Time-dependent analysis revealed a significant decrease at 24 hours in NOX4-deficient BMDCs **(Figure. 13I)**. These results demonstrate that increased IL-12p70 expression in Mtb-infected *Nox4*$^{-/-}$ BMDCs is driven by the modulation of the AKT1-GSK-3β-IRF1 signaling pathway.

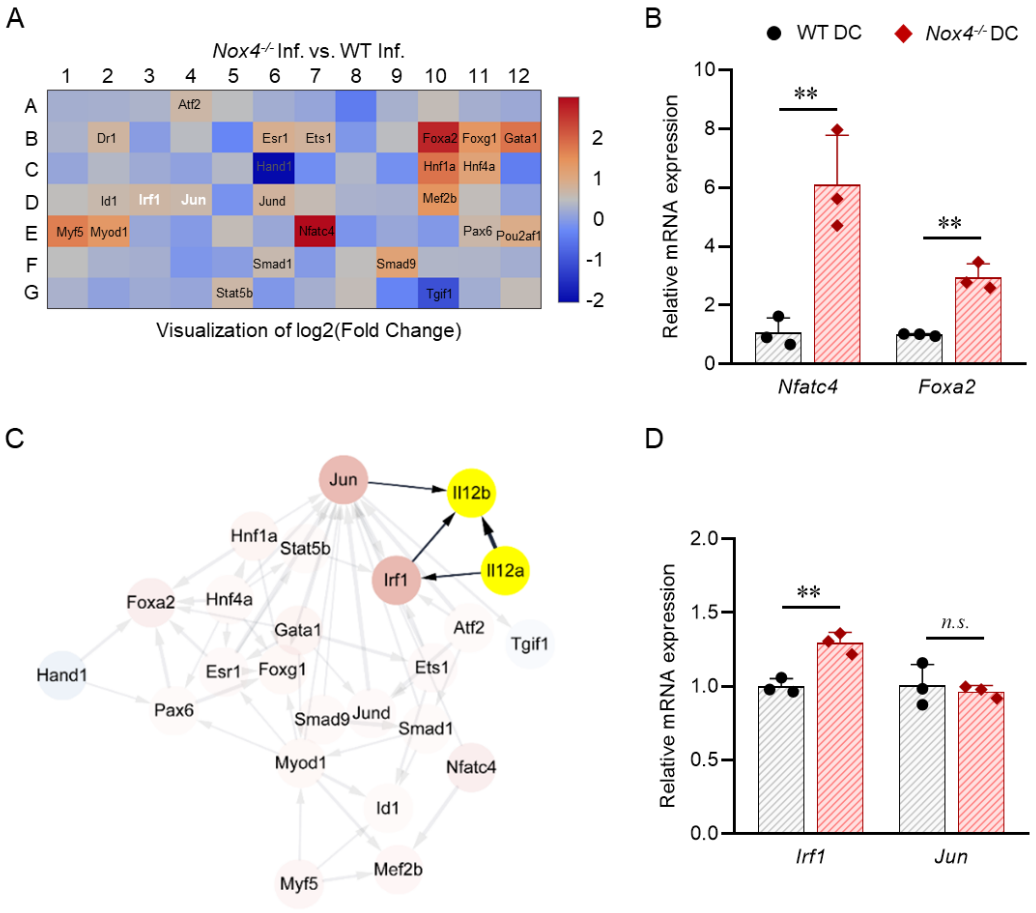

Figure 12. Comprehensive validation of PCR array data in Mtb-infected BMDCs. (A) The heatmap diagram illustrates gene expression profiling of Mtb-infected WT BMDCs and *Nox4*$^{-/-}$ BMDCs after 4 h infection according to the RT^2 profiler PCR array, which was used to screen a panel of 84 genes related with the mouse transcription factors. Red indicates higher expression levels, while blue represents lower expression levels. **(B)** Mtb-infected BMDCs (WT and *Nox4*$^{-/-}$) were analyzed at 4 h post-infection. The most upregulated genes of RT^2 Profiler^{TM} PCR array were validated by quantitative PCR and represented as the bar graphs with dot plots. **(C)** Network analysis of 24 genes interacting with *IL12a* and *IL12b* using STRING database. **(D)** Gene expression levels of *Irf1* and *Jun*,

selected for its relation to *IL12a* and *IL12b*, were measured by qPCR and represented as the bar graph with dot plots. The experiments were independently repeated at least three times, and the results from a representative experiment are presented. Data are means ± S.D. Statistical analysis was conducted by unpaired *t-test.* $^{**}p < .01$ and *n.s.*: not significant.

Table 5. List of Fold regulation for genes analyzed using the RT^2 Profiler PCR Assay

Position	Gene symbol	Fold regulation
E07	*Nfatc4*	7.99
B10	*Foxa2*	6.50
B12	*Gata1*	3.53
C10	*Hnf1a*	3.53
E01	*Myf5*	3.24
D10	*Mef2b*	2.67
B11	*Foxg1*	2.61
E02	*Myod1*	2.54
F09	*Smad9*	2.23
C11	*Hnf4a*	2.22
E12	*Pou2af1*	1.93
B06	*Esr1*	1.84
B07	*Ets1*	1.72
D06	*Jund*	1.71
B02	*Dr1*	1.68
D03	*Irf1*	1.65
A04	*Atf2*	1.62
G05	*Stat5b*	1.62
E11	*Pax6*	1.60
D04	*Jun*	1.58
D02	*Id1*	1.56
F06	*Smad1*	1.54
C06	*Hand1*	-4.08
G10	*Tgif1*	-2.09

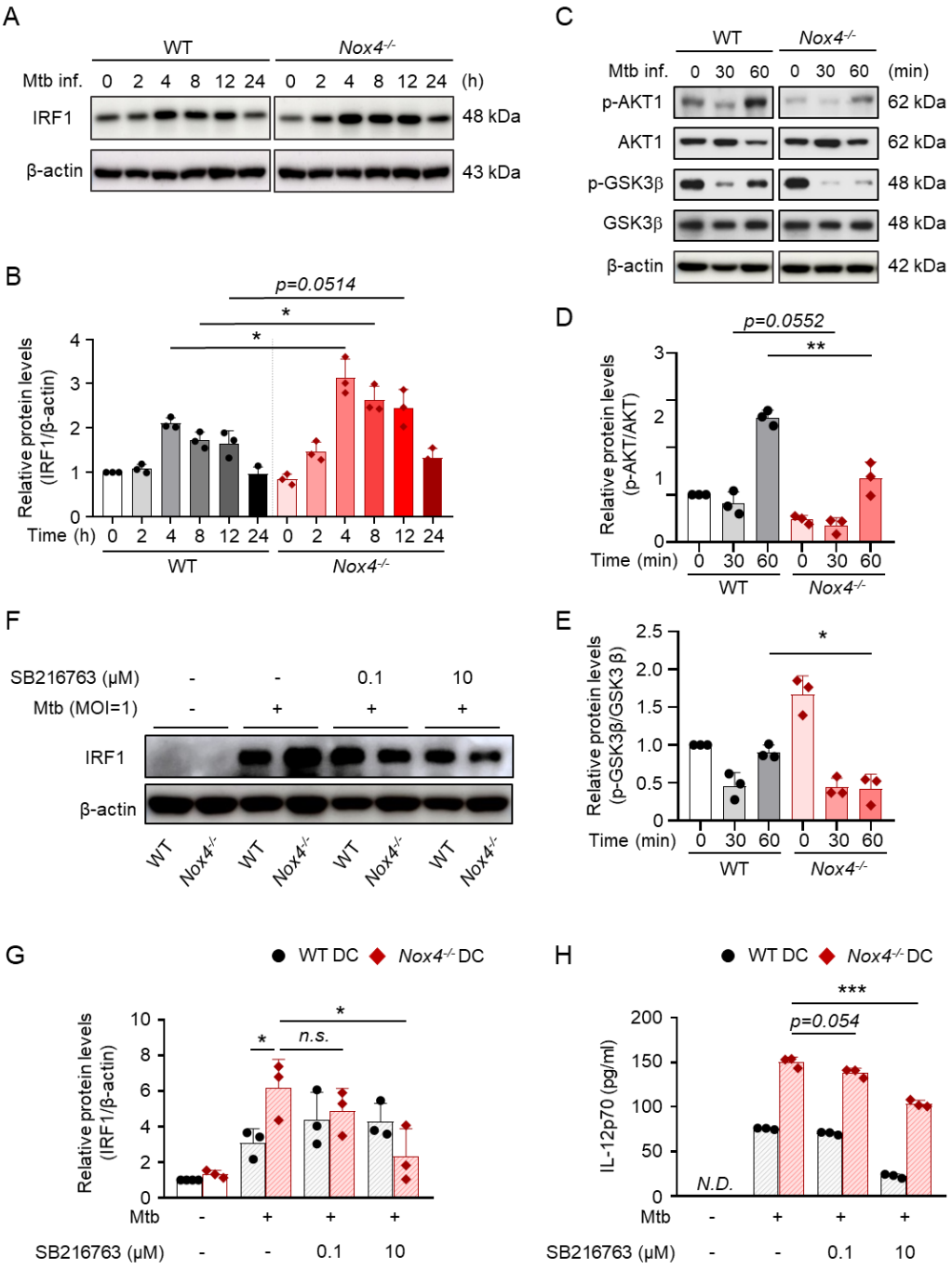

I

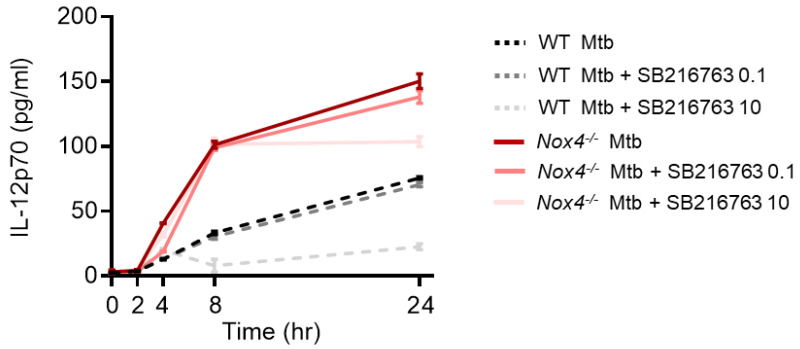

Figure 13. IL-12 upregulation in *Nox4*$^{-/-}$ BMDCs via AKT1-GSK-3β-IRF1 axis. **(A)** Representative immunoblots of the expression of IRF1 and β-actin were displayed. **(B)** Relative fold change in protein expression of IRF1 in Mtb-infected BMDCs was shown in bar graphs with dot plots. **(C)** Representative immunoblots of the expression of Phosphorylated AKT1, Phosphorylated GSK-3β and β-actin were displayed. **(D-E)** Relative fold change in protein expression of **(D)** AKT1 and **(E)** GSK-3β in Mtb-infected BMDCs were shown in bar graphs with dot plots. **(F)** BMDCs were treated with GSK-3β inhibitor (SB216763) 2 h prior to Mtb infection., and representative immunoblots of the expression of IRF1 and β-actin were displayed. **(G)** Relative fold change in protein expression of IRF1 in Mtb-infected BMDCs was shown in bar graphs with dot plots. **(H)** IL-12p70 production was measured in the supernatants of Mtb-infected BMDCs after 24 h by ELISA and presented as bar graphs with dot plots and **(I)** time-dependent response of IL-12p70 in Mtb-infected BMDCs was determined by ELISA and visualized through line graphs. The experiments were independently repeated at least three times, and the results from a representative experiment are presented. Data are shown as means ± S.D. Statistical analysis was conducted by unpaired *t-test*. *$p < .05$, **$p < .01$, and *n.s.:* not significant. Abbreviation: Inf., Infection

4. Discussion

In the current study, we aimed to investigate the potential role of NOX4 in adaptive immune responses during Mtb infection and underlying mechanisms *in vivo* and *in vitro*. To comprehensively assess the involvement of NOX4 across sexes, *in vivo* experiments were meticulously conducted four times, encompassing both male and female mice. Strikingly, *Nox4*$^{-/-}$ mice exhibited a significant reduction in bacterial burden and lung pathology compared to WT mice, irrespective of sex. Given the higher prevalence of TB in males,[37-39] our investigation primarily focused on elucidating the role of NOX4 in male mice.

Under Mtb-infected conditions, the number of CD45^{+} leukocytes, DCs and T cells was also increased in the lung of *Nox4*$^{-/-}$ mice, accompanied by a significant elevation in IFN-γ levels, suggesting that NOX4 deficiency may influence both immune cell composition and function during Mtb infection. As previously reported that DCs act as key mediators in recognizing and presenting antigens, orchestrating T cell activation to combat TB infection.[40] Our study demonstrated that NOX4 deficiency enhances DC activation, leading to heightened CD4^{+} T cell responses. *Nox4*$^{-/-}$ BMDCs exhibited increased IL-12 production, driving elevated IFN-γ producing CD4^{+} T cells. These findings highlight the absence of NOX4 could bolster the immune responses of DCs in the context Mtb infection, suggesting a potential avenue for improved TB control.

Our study showed that *Nox4*$^{-/-}$ BMDCs enhanced the CD4^{+} T cell-derived IFN-γ production, with this effect not attributed to *Nox4*$^{-/-}$ T cells themselves. IFN-γ is a critical cytokine in the host defense against Mtb infection by activating macrophages and recruiting additional immune cells.[41,42] Previous studies have shown that Mtb uses several mechanisms to inhibit DC maturation and, specifically, suppress IL-12 secretion, thus impairing the development of protective T-cell response.[43,44] The results highlighted the role of NOX4 in regulating IL-12 and activating immune responses in DCs during Mtb infection.

In *Nox4*$^{-/-}$ BMDCs, reduced AKT1 phosphorylation was linked to increased IL-12 secretion. Previous studies reported that AKT1 activation inhibits GSK3β activity by phosphorylating serine 9, reducing IL-12 secretion.[45,46] Conversely, GSK3β activation promotes IRF-1 degradation by phosphorylating its T181 residue, and IRF-1 is crucial for IL-12 production in DCs.[35,36] Although the detailed mechanistic hierarchy among GSK3β, IRF1, and IL-12 regulation remains incompletely defined, our data suggest that IRF1 expression is modulated in response to changes in GSK3β activity, supporting a sequential link between these factors in IL-12 production. We exhibited that *Nox4*$^{-/-}$ BMDCs showed reduced GSK3β phosphorylation and increased IRF-1 expression during Mtb infection. This suggests that lower AKT1 phosphorylation in *Nox4*$^{-/-}$ BMDCs reduces GSK3β phosphorylation, increasing IRF1 expression, and enhancing IL-12 production, which drives a protective T cell response. These findings align with the observation that *Nox4*$^{-/-}$ BMDCs are more effective at promoting $CD4^+$ T cell responses and IFN-γ production.

This study has three limitations. First, given that NOX4 is known to influence the differentiation of various immune cell populations, there may be baseline differences in immune cell composition between WT and *Nox4*$^{-/-}$ mice.[47,48] We did not directly assess these differences, and we could not rule out the possibility that such variations contributed to our findings. Future studies are needed to investigate this aspect. Second, while our findings demonstrate that IL-12p70 is a key mediator of enhanced Th1 activation in *Nox4*$^{-/-}$ BMDCs. IFN-γ production remained higher in T cells co-cultured with *Nox4*$^{-/-}$ DCs compared to WT DCs even after IL-12 neutralization. One possible explanation is that the fixed concentration of neutralizing antibody may not have been sufficient to block the elevated baseline IL-12p70 in *Nox4*$^{-/-}$ DCs. Alternatively, additional IL-12-independent mechanisms, such as cytokine profiles or increased co-stimulatory signaling, may have contributed to the residual Th1 response. Further investigation is warranted to elucidate these pathways and fully define the immunoregulatory role of NOX4. Third, the activation of the PI3K/Akt pathway by NOX4 is consistent with previous studies conducted in various cellular contexts, such as non-small cell lung cancer and hepatic stellate cells.[23,49,50]

However, these studies described this activation as ROS-dependent. In immune cells, the role of NOX4 in ROS generation remains controversial and appears to vary depending on the type of stimulus and cellular context.[22,51] For instance, Lee *et al.* demonstrated that NOX4 knockdown or overexpression altered ROS levels in macrophages stimulated with oxidized LDL.[51] In contrast, Helfinger *et al.* reported that NOX4-deficient macrophages exhibited increased ROS production following LPS and IFN-γ stimulation, which was attributed to compensatory upregulation of NOX2, along with enhanced NF-$_k$B activation and proinflammatory cytokine expression.[22] These conflicting findings highlight the complexity of NOX4-mediated signaling and suggest that NOX4's contribution to ROS production is context- and stimulus-dependent. In our study, however, we observed NOX4-dependent Akt activation without a significant difference in ROS levels between WT and *Nox4*$^{-/-}$ BMDCs, suggesting a ROS-independent mechanism in this context. The precise role of ROS in this signaling cascade remains unclear and warrants further investigation.

In summary, our study demonstrates that NOX4 deficiency enhances IL-12 production via the AKT-GSK3β-IRF1 pathway in DCs, boosting IFN-γ production in CD4$^+$ T cells and aiding in Mtb control. These results emphasize the importance of NOX4 in regulating the interactions between DCs and T cells in the context of Mtb infection. Targeting NOX4 with inhibitors could promote Th1 responses, offering a potential strategy for TB control and vaccine development. Further research on NOX4 inhibitors in DCs could aid TB vaccine adjuvant development.

5. Conclusion

Collectively, our study revealed that NOX4 negatively regulates IL-12 production in Mtb-infected DCs, suppressing Th1-mediated immunity. Its absence enhances Th1 responses, improves immune control of Mtb, and boosts BCG vaccine efficacy. Targeting NOX4 may improve tuberculosis outcomes by strengthening host immunity.

Chapter II

Differential regulation of airway inflammation by NOX4 deficiency and colchicine in asthma mouse model

1.Introduction

Asthma is a chronic and heterogeneous airway disorder that affects over 300 million individuals globally.[52] It is defined by airway obstruction, bronchial hyper responsiveness, and persistent inflammation, often involving the infiltration of diverse immune cells into pulmonary tissue.[53] The disease arises from the activation and recruitment of immune cell populations, such as eosinophils, neutrophils, and T lymphocytes, which contribute to variable clinical phenotypes.[54] Among these, eosinophilic asthma is the most prevalent subtype, typically associated with type 2 (Th2)-mediated immune responses and elevated eosinophil counts in the airways.[55] Th2 cells orchestrate this response by producing cytokines such as IL-4, IL-5, and IL-13, which collectively promote the recruitment and survival of eosinophils, excessive mucus secretion, and bronchoconstriction.[56] In particular, IL-5 and IL-13 are central to the regulation of eosinophil maturation, activation, and trafficking.[56] Gaining a deeper understanding of the cytokine networks and immune pathways involved in Th2-dominant asthma is critical for developing more selective and effective therapeutic interventions.[57]

Reactive oxygen species (ROS) have emerged as key regulators of airway inflammation and remodeling in asthma. NADPH oxidase 4 (NOX4) is a major source of ROS in epithelial cells, fibroblasts, and immune cells within the respiratory tract.[58] In the context of asthma, oxidative stress exacerbates inflammatory processes by amplifying cytokine signaling, activating immune cell responses, and inducing epithelial injury.[59] Although the role of NOX4 has been extensively studied in fibrotic and cardiovascular conditions, its

precise involvement in asthma pathogenesis remains insufficiently defined, and its potential as a therapeutic target in allergic airway inflammation is yet to be fully explored.[60]

Inhaled corticosteroids (ICS) are currently regarded as the mainstay of asthma treatment owing to their anti-inflammatory efficacy and are often prescribed in combination with bronchodilators.[61] However, their therapeutic efficacy varies considerably depending on the asthma endotype.[54] Prolonged ICS usage has been associated with systemic side effects, including adrenal suppression, osteoporosis, and metabolic complications.[62] Moreover, corticosteroids generally exert broad-spectrum immunosuppressive effects rather than specifically targeting Th2-driven inflammation.[54] This lack of selectivity may increase susceptibility to infections and limit treatment effectiveness in patients with complex or steroid-resistant phenotypes. These challenges highlight the need for novel or adjunctive treatments that can modulate pathogenic immune responses with greater precision and improved safety profiles.[57]

Although recent developments in biologic therapies have provided new treatment options, the discovery and approval of novel drugs remains a lengthy and costly process.[57,63] In this context, drug repurposing the application of existing drugs for new indications has become an increasingly attractive approach for expanding treatment strategies.[57]

Colchicine, a long-established non-steroidal anti-inflammatory drug, has traditionally been used to manage gout and familial Mediterranean fever, and is also prescribed off-label for several inflammatory conditions, including vasculitis, Paget's disease, and Behçet's disease.[64] Its primary mechanism involves the inhibition of microtubule assembly through binding to tubulin, thereby altering intracellular transport and structural dynamics.[65] Given that microtubules are integral to cytokine release, vesicular trafficking, and immune cell motility, colchicine exerts broad anti-inflammatory effects by disrupting these cellular processes.[66] Owing to its oral bioavailability, favorable safety profile, and low cost, colchicine has been investigated as a potential repurposed treatment in diseases such as COVID-19, coronary artery disease and tuberculosis.[67-69] Moreover, colchicine reduced

NOX4 expression in an abdominal aortic aneurysm (AAA) mouse model and suppressed pro-inflammatory cytokines to alleviate inflammation.[70] Nevertheless, its utility in asthma remains largely underexplored.

In this study, we aimed to evaluate the immunoregulatory potential of NOX4 deletion and colchicine treatment in murine models of asthma. By comparing genetic and pharmacological interventions targeting key immunological pathways, we investigated whether NOX4 inhibition or treatment with a non-steroidal anti-inflammatory agent such as colchicine could mitigate Th2-mediated airway inflammation and provide alternative or adjunctive benefits to corticosteroids in allergic asthma.

2. Material and methods

2.1. Animals and ethics statement

Female C57BL/6 and BALB/c mice (aged 5 weeks) were purchased from Orient Bio (Gyeonggi-do, South Korea), and age-matched female *Nox4*$^{-/-}$ mice were kindly provided by Dr. Yun Soo Bae (Ewha Womans University, Seoul, South Korea) and Dr. Ji-Hwan Ryu (Yonsei University, Seoul, South Korea). The mice were housed in a specific pathogen-free conditioned facility and provided water and a sterile commercial diet ad libitum at a controlled environment (24±1 ℃, 50±5 % humidity and 12 hr day / night cycle). The mice were allowed to adapt for one week before using in any experiments. All procedures were approved by the Ethics Committee and Institutional Animal Care and Use Committee of the Yonsei University College of Medicine (Permission number: 2022-0275) and Hallym University Medical Center (Permission number: HMC 2023-3-0814-39).

2.2. Generation of OVA-loaded BMDCs

Bone marrow-derived dendritic cells (BMDCs) were generated from bone marrow (BM) cells following the standard protocol described in Chapter I. On day 8 of culture, BMDCs were collected and seeded into 24-well plates at a density of 1×10^6 cells per well. The cells were then incubated for 24 hours with 500 μg/ml of OVA protein. On day 9, OVA-pulsed BMDCs were harvested for subsequent use.

2.3. *In vivo* asthma modeling and colchicine treatment

To establish an asthma model using adoptive transfer of ovalbumin (OVA)-pulsed dendritic cells (DCs), the allergen sensitization and challenge protocol was adapted with modifications based on previously reported methods.[71] Mice were sensitized on days 0 and 14 via intraperitoneal (i.p.) injection of 50 μg of ovalbumin (OVA; Sigma-Aldrich, St. Louis, MO, USA) mixed with 1.32 mg of aluminum hydroxide gel (alum; Sigma) in 200 μl of dPBS. From day 21 to 25, mice received daily intravenous (i.v.) injections of 1×10^7

bone marrow-derived dendritic cells (BMDCs) loaded with 500 μg of OVA, administered through the tail vein in a final volume of 200 μl.

For establishing conventional asthma mouse model, Balb/c female mice were sensitized on day 0, 14 through i.p. injection of 50 μg of ovalbumin and 1.32 mg of aluminum hydroxide gel in 200 μl of dPBS. And then the mice were aerosol challenged with 4 % OVA in 4 ml PBS for 30 min in a day for consecutive 5 days starting from day 21. Five groups of animals, Control, negative control group; OVA, OVA induced asthma with PBS group; OVA + Col 0.1 mg/kg, OVA induced asthma with 0.1 mg/kg colchicine group; OVA + Col 1 mg.kg, OVA induced asthma with 1 mg/kg colchicine group; OVA + Dexa 10 mg/kg, OVA induced asthma with treatment of dexamethasone as positive control group, were used for each experiment. Colchicine (Sigma) was dissolved in dimethyl sulfoxide at 250 mg/ml and stored in –20 ℃, as stock solution. Dexamethasone (Sigma) was dissolved in autoclaved distilled water at 10 mg/ml and stored in –20 ℃, as stock solution. For oral administration in vivo, stock solution of colchicine and dexamethasone were further diluted with autoclaved tap water. For colchicine and dexamethasone treatment, mice were administered drugs orally once a day for consecutive 6 days starting from a day before the first challenge. Mice were sacrificed at 24 hr following the last challenge and analyzed.

2.4. Preparation of *In vivo* sample

After completing the experiment, blood was collected from the mice using orbital puncture technique and centrifuged at 2,000 rpm for 10 min to obtain serum. bronchoalveolar lavage fluid (BALF) was collected by inserting a catheter and instilling 2ml of dPBS containing 0.05mM EDTA. And then BALF was centrifuged at 2,000 rpm for 10 min. The serum and BALF sample were stored in under –30 ℃ for immunological analysis. After perfusing the mouse heart 10ml of dPBS, the lung tissue was kept in dPBS at 4 ℃ until the next step. The left lung lobe was used for histological analysis and the right lobe was used for flow cytometric and molecular analysis.

2.5. Histological analysis of lung tissue

To evaluate lung inflammation and goblet cell hyperplasia, lung tissue (left lung lobe) was fixed with 4 % paraformaldehyde solution for over 24 h and cut into 4 pieces and embedded in paraffin for sectioning. The tissue blocks were sectioned and stained with hematoxylin and eosin (H&E) and periodic acid-schiff (PAS) solution. After staining, lung inflammation and goblet cell hyperplasia were analyzed by using a previously reported semiquantitative scoring system[77]. Briefly, lung tissues were randomly captured at 100X magnification for H&E scoring and 200X magnification for PAS scoring. H&E scoring was performed based on a five-point scoring system (0, no cell; 1, a few cells; 2, a ring of cells 1 cell layer deep; 3, a ring of cells 2-4 cell layer deep; and 4, a ring of cells >4 cells layer deep). PAS scoring was performed based on a five-point grading system (0, no goblet cells; 1, <25%; 2, 25–50%; 3, 50–75%; and 4, >75%). 16 images were captured for each mouse, and the average score was calculated and analyzed. The average scores for H&E and PAS were defined as the value for the lung inflammation and goblet cell hyperplasia.

2.6. Single cell preparation from lung tissue

The lung tissue was finely chopped to obtain single cells. Collagenase cocktail (0.1% collagenase II (Worthington-Biochem), 0.1 % MgCl2 (Sigma), 0.1 % CaCl2 (Sigma), 2 % Fetal Bovine Serum (FBS, Biowest), 1 % Penicillin-Streptomycin solution (P/S, Biowest) in RPMI 1640 medium (Biowest) was treated and incubated at 37 ℃, 5 % CO2 for 20-30 min to digest the lung tissue collagen. After digestion with collagenase cocktail, lung tissue was meshed by using 40 μm strainer. And then, the single cells were harvested after centrifugation at 1,800 rpm for 3 min. ACK lysis buffer (Gibco) was applied to lyse and remove red blood cells.. Then, the single cells were harvested after centrifugation at 1,800 rpm for 3 min and resuspended in RPMI 1640 media containing 10 % FBS and 1 % P/S for seeding $1X10^6$ cells in 200 μl per well.

2.7. Restimulation for analysis of T cell cytokine release

The lung cells from the right lobe were cultured in RPMI 1640 medium supplemented with 1 % P/S and 10 % FBS at 37 ℃ 5 % CO_2. And then the supernatants were collected 72 hr after re-stimulation with OVA protein (10 μg /ml) in separated single cells from lung tissue and stored at under -30 ℃.

2.8. Enzyme-linked immunosorbent assay (ELISA) for cytokine analysis

For analyzing Th cell response, cytokine measurement was conducted. The OVA re-stimulation-cultured cell supernatants and BALF were quantified by using mouse uncoated sandwich ELISA kits. The levels of IL-5, IL-13, IL-17AF, IFN-γ were measured following the manufacturer's instructions. Serum antigen-specific antibody titers were quantified by indirect ELISA. Briefly, serum was diluted (1:50 for OVA-specific IgE and 1:10,000 for OVA-specific IgG1) and added to a plate coated with OVA (1 mg/ml for IgE and 10 ug/ml for IgG1). The antibody titers were then detected with biotin-conjugated rat anti-mouse IgE (BD Pharmingen) or biotin-conjugated rat anti-mouse IgG1 (BD Pharmingen), followed by incubation with HRP-conjugated avidin. TMB solution was used for color development and absorbance was measured at 450 nm.

2.9. Flow cytometry for lung infiltrated cell analysis

For analysis of lung infiltrated immune cell, single cells from lung and BALF were stained with listed antibodies. To blocking Fcγ receptors, single cells were blocked with anti-CD16/CD32 for 15 min at 4 ℃. Surface molecules were stained with fluorochrome-conjugated anti-CD45, anti-CD11b, anti-Ly6G, anti-Siglec-F antibodies for 30 min at 4 ℃. Once surface molecule labeling was complete, cells were treated with IC Fixation Buffer (Invitrogen) for fixation. The stained cells were analyzed by cytoflex 2L6C flow cytometer (Beckman-Coulter) and FlowJo software (V.10.4, Tree Star, Inc.).

2.10. Statistical analysis

Four to five mice were sacrificed per group in each experiment. Data in the graphs are represented as the mean value with the standard error of the mean (SEM) and the standard deviation (S.D.). Comparisons between groups were determined by one-way ANOVA with Tukey's multiple comparisons test using GraphPad Prism version 8.0. Statistical significance was determined as not significant (*n.s.*); *$p < 0.05$; **$p < 0.01$; ***$p < 0.001$, ****$p < 0.0001$.

3. Results

3.1. NOX4 deficiency attenuates airway inflammation and mucus production in a BMDCs-induced asthma model

To investigate the role of NOX4 in asthma, we established an asthma model by intravenously injecting OVA-pulsed bone marrow-derived dendritic cells (BMDCs) into wild-type (WT) and NOX4 knockout (*Nox4*$^{-/-}$) mice **(Figure.1A)**. Histological analysis of lung tissue was performed to assess airway inflammation and mucus production. Inflammatory scores showed significant reduction in *Nox4*$^{-/-}$ mice compared to WT mice **(Figure.1B)**. Next, to evaluate goblet cell hyperplasia, we conducted periodic acid-schiff (PAS) staining. Mucus production slightly decreased in *Nox4*$^{-/-}$ mice than WT mice **(Figure.1C)**. These results indicate that NOX4 deficiency could attenuate airway inflammation and mucus hypersecretion, suggesting a possible protective effect against asthma-associated histological features.

A

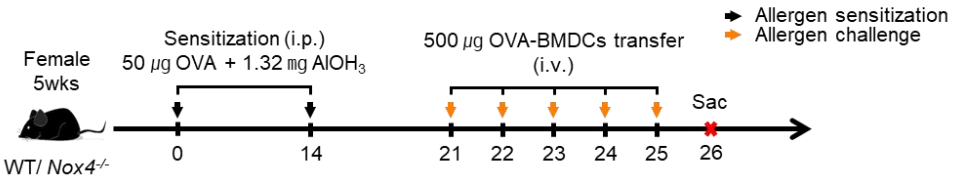

B

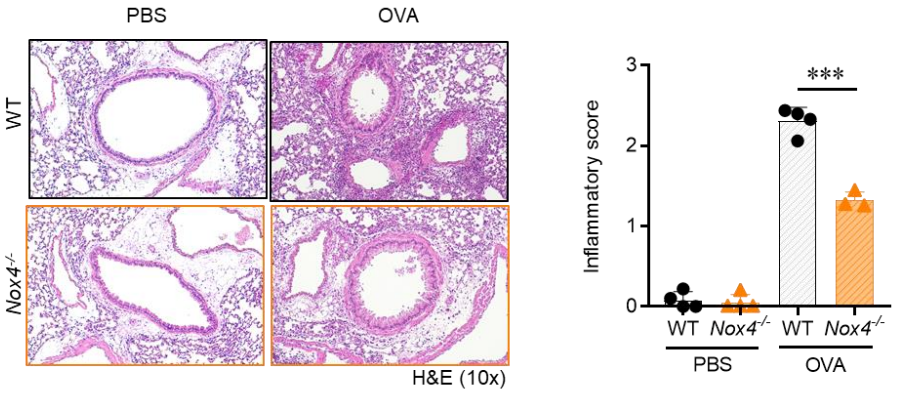

C

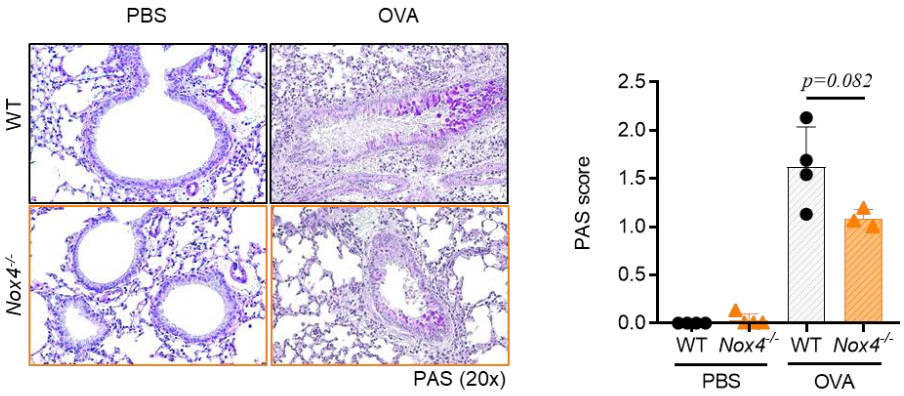

Figure 1. Reduced airway inflammation and mucus secretion in *Nox4*$^{-/-}$ mice. (A) Experimental scheme of asthma induction using OVA-pulsed bone marrow-derived dendritic cells (BMDCs) in WT and *Nox4*$^{-/-}$ mice. **(B)** Representative histological imaged of lung sections stained with hematoxylin and eosin (H&E) from WT and *Nox4*$^{-/-}$ mice. **(C)** Representative histological imaged of lung sections stained with periodic acid-schiff (PAS) from WT and *Nox4*$^{-/-}$ mice. Data are means ± S.D. Statistical analysis was conducted by unpaired *t-test*. ***$p < .001$.

Abbreviation: OVA, Ovalbumin; $AlOH_3$, Aluminum hydroxide; WT, C57BL/6 wild-type mice; *Nox4*$^{-/-}$, NOX4-deficient mice.

3.2. The NOX4 deficiency modulates immune cell composition without suppressing Th2 cytokine responses.

To further explore how NOX4 deficiency impacts immune responses in asthma, we examined both lung infiltrated immune cell population and cytokine production in WT and *Nox4*$^{-/-}$ mice. We assessed the composition of infiltration immune cell in lung by flow cytometry. While the total number of CD45^{+} immune cells was similar, we found a significant increase in neutrophils, dendritic cells (DCs), and macrophages in the lungs of *Nox4*$^{-/-}$ mice compared to WT mice **(Figure. 2)**. This increase in DCs was also evident in the tuberculosis model, indicating a shared immunological feature of NOX4 deficiency. Notably, the number of eosinophils that play a key role in asthma was unchanged **(Figure. 2)**. Subsequently, to assess whether the increased number of dendritic cells modulated T cell responses, we subsequently measured cytokine levels. Lung single-cell suspensions were prepared and stimulate *ex vivo* with 10 μg/ml of OVA for 24 hours. Analysis of culture supernatant revealed no significant differences in cytokine levels **(figure. 3A)**. Consistently, cytokine levels measured in BALF showed no differences in IL-5, IL-13 **(Figure. 3B)**. In mediastinal lymph nodes (MLNs), IL-5 was marginally reduced in *Nox4*$^{-/-}$ mice, while other cytokines remained unchanged **(Figure. 3C)**. Together, these findings indicate that NOX4 deficiency does not significantly affect adaptive Th2 cytokine responses but induces a notable shift toward innate immune cell infiltration within the lung, suggesting an alternative immunological pathway contributing to asthma attenuation.

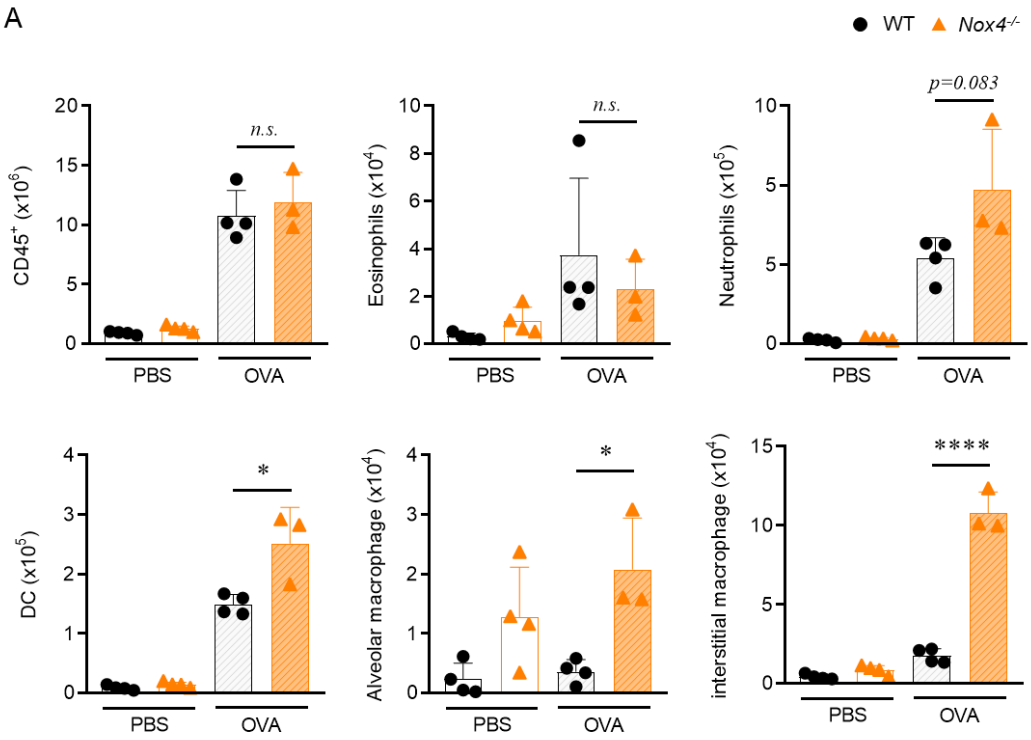

Figure 2. The NOX4 deficiency alters innate immune cell infiltration without affecting eosinophil numbers in the lungs. Flow cytometric analysis was performed to determine the number of immune cell subsets in the lungs of WT and *Nox4*$^{-/-}$ mice after OVA-pulsed BMDC-induced asthma. Quantitative analysis of total immune cells (CD45^{+}), eosinophils (Siglec-F^{+}CD11c^{-}), neutrophils (CD11b^{+}Ly6G^{+}), dendritic cells (CD11c^{+}MHCII^{+}), alveolar macrophages (Siglec-F^{+}CD11c^{+}), and interstitial macrophages (CD11b^{+}F4/80^{+}) are presented. Data are means ± S.D. Statistical analysis was conducted by unpaired *t-test*. *p < .05, ****p < .0001 and n.s.: not significant.

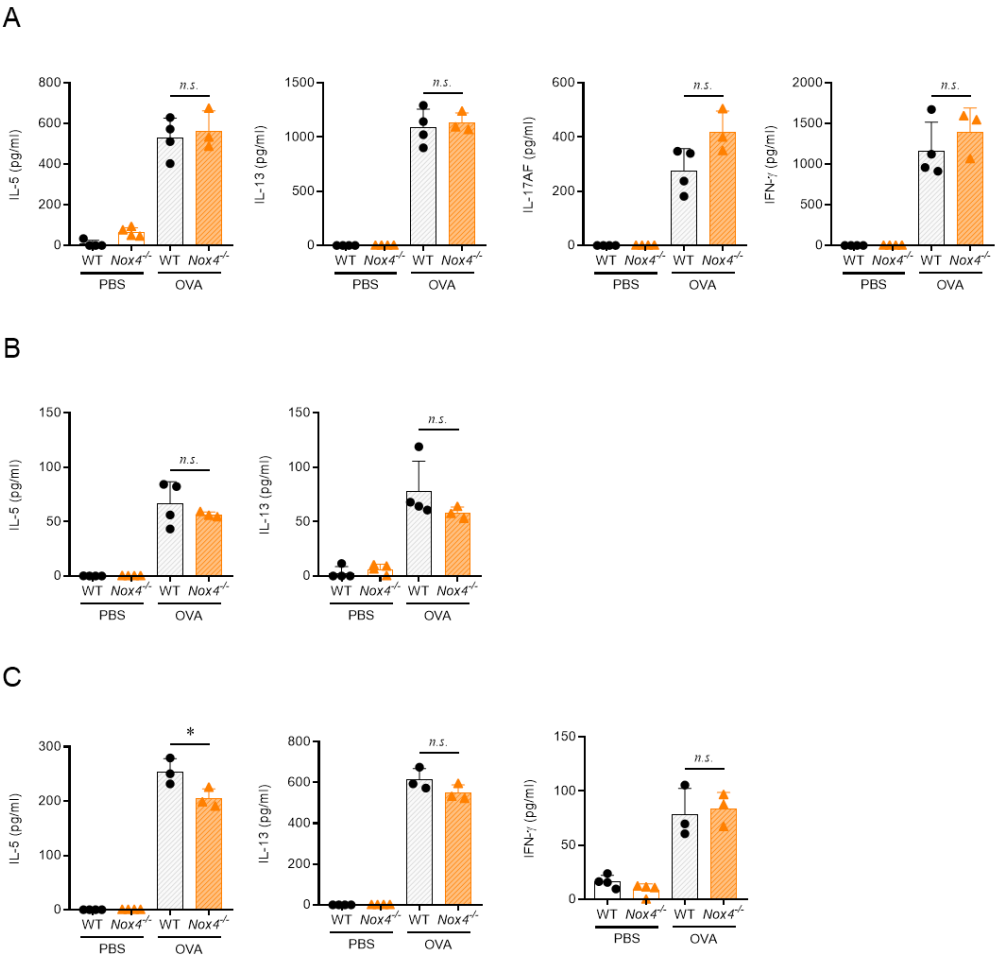

Figure 3. The NOX4 deficiency does not significantly alter Th2 cytokine production in lung tissue, BALF, and MLNs. Cytokine levels (IL-4, IL-5, IL-13) were measured by ELISA in **(A)** lung single-cell suspensions stimulated *ex vivo* with OVA (10 μg/ml) for 24 hours, **(B)** bronchoalveolar lavage fluid (BALF), and **(C)** Supernatants were collected from MLN cells that had been *ex vivo* stimulated with 10 μg/ml OVA for 24 hours. Data are means ± S.D. Statistical analysis was conducted by unpaired *t-test*. *p < .05, and n.s.: not significant.

3.3. Colchicine treatment suppressed IL-4 and IL-13 secretion in activated CD4$^+$ T cells

To determine whether colchicine directly affects Th2 cytokine production, we isolated CD4$^+$ splenic T cells from Balb/c mice and stimulated them *ex vivo* with 1x concanavalin A (ConA) in the presence or absence of colchicine. Colchicine was selected due to its known inhibitory effects on cytokine secretion by interfering with microtubule polymerization, thereby modulating immune cell function and Th2-mediated inflammation.[73] To assess cytokine production, ELISA was performed on supernatants collected 24 hours after stimulation. Colchicine treatment significantly reduced the secretion of IL-4 and IL-13, key Th2 cytokines involved in asthma pathogenesis, compared to the ConA only stimulated control group **(Figure. 4A)**. In contrast, IL-10, IFN-γ levels were not significantly altered by colchicine treatment **(Figure. 4A)**. Furthermore, a decreasing trend in proliferation was observed following colchicine treatment **(Figure. 4B)**. These findings indicate that colchicine selectively suppresses specific Th2 cytokines (IL-4 and IL-13) in activated CD4$^+$ T cells, potentially as a result of reduced T cell proliferation. This supports its potential utility in modulating eosinophilic inflammation associated with asthma.

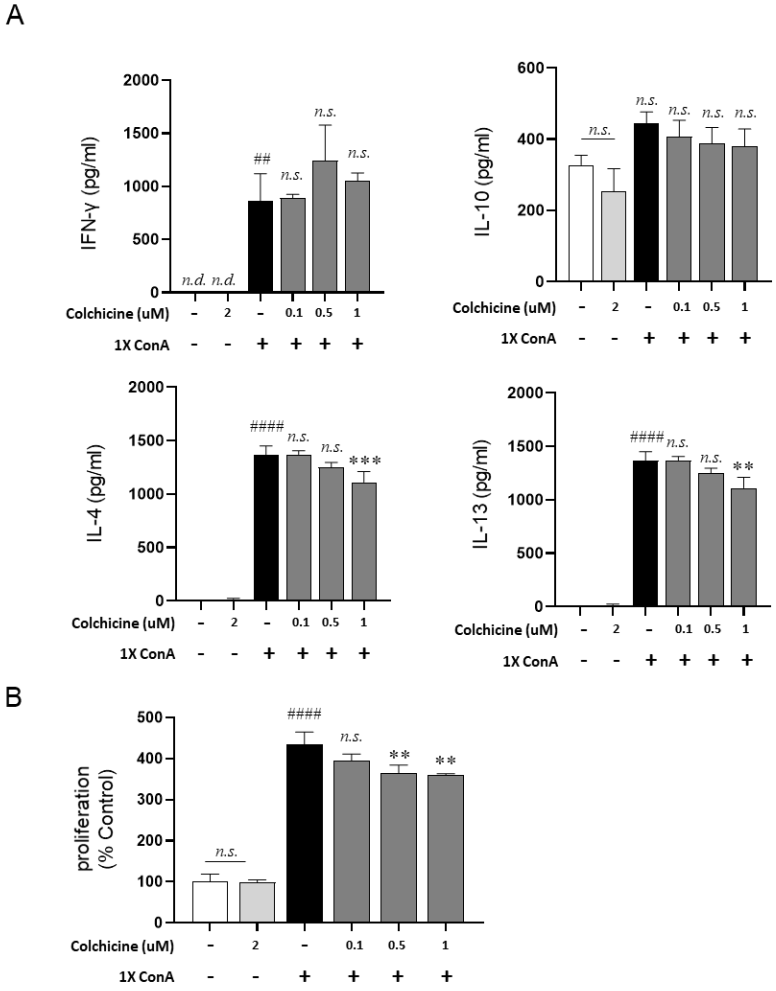

Figure 4. Colchicine treatment reduces Th2 cytokine production in CD4⁺ T cells stimulated with ConA. Splenic CD4⁺ T cells isolated from Balb/c mice were stimulated *ex vivo* with 1x concanavalin A in the presence or absence of colchicine (0.1, 0.5, 1 μM) for 24 hours. Cytokine levels of **(A)** IL-4, IL-13, IFN-γ, IL-10 in culture supernatants were measured by ELISA. **(B)** proliferation was conducted by CCK-8 assay. Data are means ± S.D. Statistical analysis was conducted by unpaired *t-test*. ***p* < .01, ****p* < .001, *****p* < .0001, and n.s.: not significant.

3.4. Colchicine treatment reduced the infiltration of inflammatory cells in lung and BALF during OVA induce asthma mouse model

To assess the effect of colchicine in the development of allergic airway inflammation, we induced conventional asthma. A mouse model of conventional asthma was established using sensitization and aerosol challenge with OVA **(Figure.5A)**. Two different doses of colchicine (0.1 mg/kg or 1 mg/kg) were administered orally on one day before challenge for six consecutive days **(Figure.5A)**. In this model, many features of asthma were represented including infiltration of eosinophils. Eosinophils are markedly increased in the lungs and upper airway tissues during allergic inflammation conditions.[74] Eosinophils are known to migrate with other inflammatory cells and are believed to contribute to mucus production and bronchoconstriction in the respiratory system.[74] Infiltration of inflammatory cells in the airway was assessed by flow cytometry **(Figure.5B-C)**. Notably, treatment with colchicine significantly decreased eosinophil infiltration in the lung compared to OVA challenged mice group **(Figure.5B)**. However, no differences were seen in neutrophil infiltration in the lung compared to OVA challenged mice group **(Figure.5B)**. Similarly, Colchicine treatment group had statistically significant reduction in eosinophils in BALF compared to OVA challenged mice group, whereas there were no significant differences in neutrophils **(Figure. 5C)**. These experiments show that colchicine treatment decreased eosinophil infiltration and suggest that colchicine diminished allergic airway inflammation at least in part.

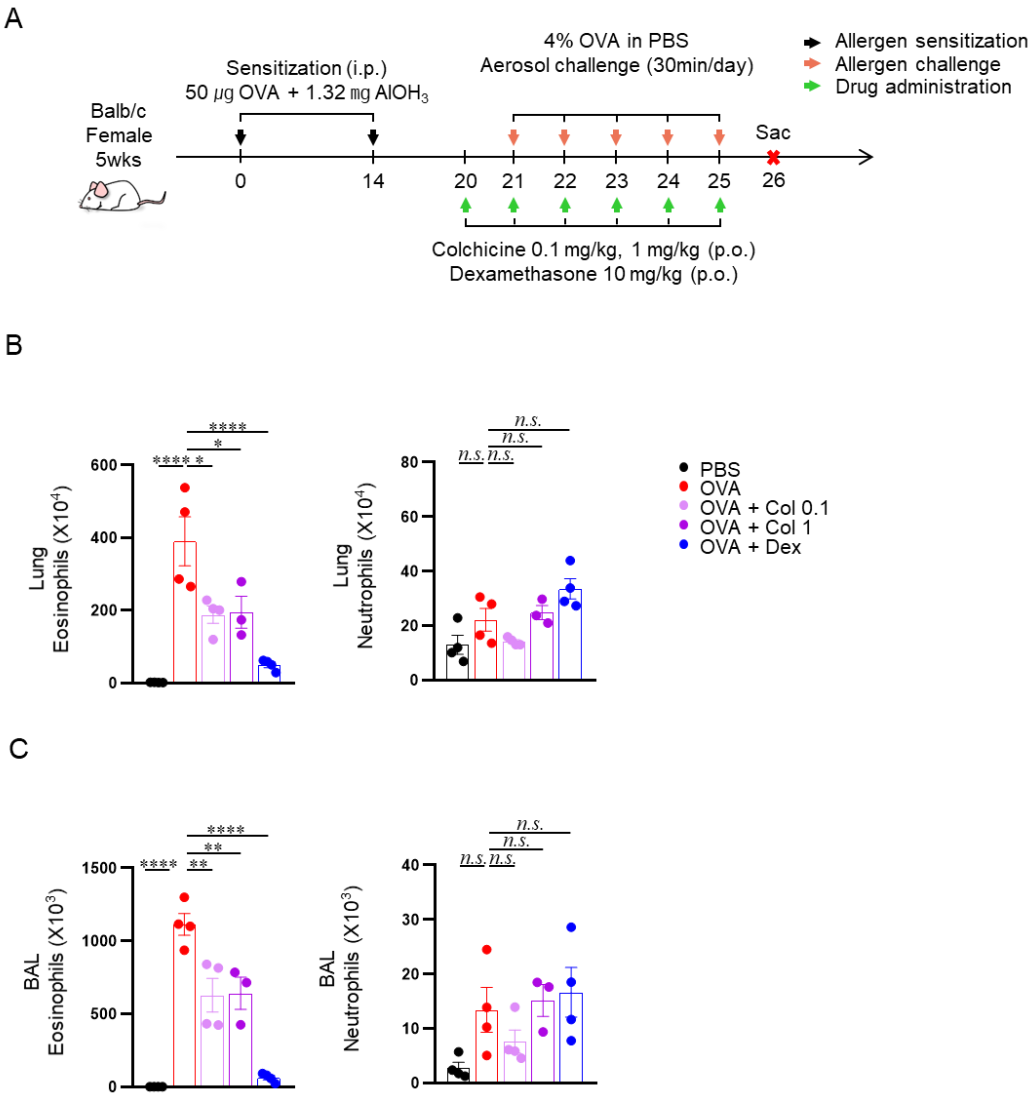

Figure 5. The infiltration of inflammatory cells in lung after colchicine treatment on mouse model of asthma. (A) Ovalbumin (OVA) sensitization, challenge, and colchicine treatment mouse model. Mice were sensitized with OVA and alum, then challenged with OVA aerosol for consecutive 5 days. **(B)** The number of eosinophils and neutrophils infiltrating the lung was quantified by flow cytometric analysis. **(C)** Cell numbers of

infiltrated eosinophils and neutrophils in BALF as determined by Flow cytometry. Data are means ± SEM. Statistical analysis was conducted by one-way ANOVA with Tukey's multiple comparisons test. *$p < .05$, **$p < .01$, ****$p < .0001$, and *n.s.*: not significant.

3.5. Colchicine treatment does not alleviate the histological aspects of lung tissue and OVA specific antibody production in OVA induced asthma mouse model

We then determined the lung tissue inflammation and mucus production, both characteristic features of asthma, by histological analysis. The lung tissue inflammation was confirmed by examining lung tissue sections to detect inflammatory cell infiltration using hematoxylin-eosin staining **(Figure.6A)**. There were no significant differences in colchicine treatment group compared to OVA challenged mice group **(Figure.6A)**. The mucus production was analyzed by using periodic acid Schiff staining **(Figure.6B)**. Colchicine treatment group had no statistically significant reduction in mucus production compared to OVA challenged group, but slightly decreased tendency was observed in colchicine 1 mg/kg treatment group **(Figure.6B)**. Next, OVA-specific IgE and IgG_1 level in sera, another feature of asthma, were evaluated. Notably, OVA-specific IgE levels significantly reduced in the colchicine 0.1 mg/kg treatment group compared to the OVA challenged group, whereas IgG_1 levels showed no significant differences **(Figure.6C)**. Collectively, these results suggest that colchicine treatment may partially alleviate certain features of asthma, such as OVA-specific IgE production and mucus secretion.

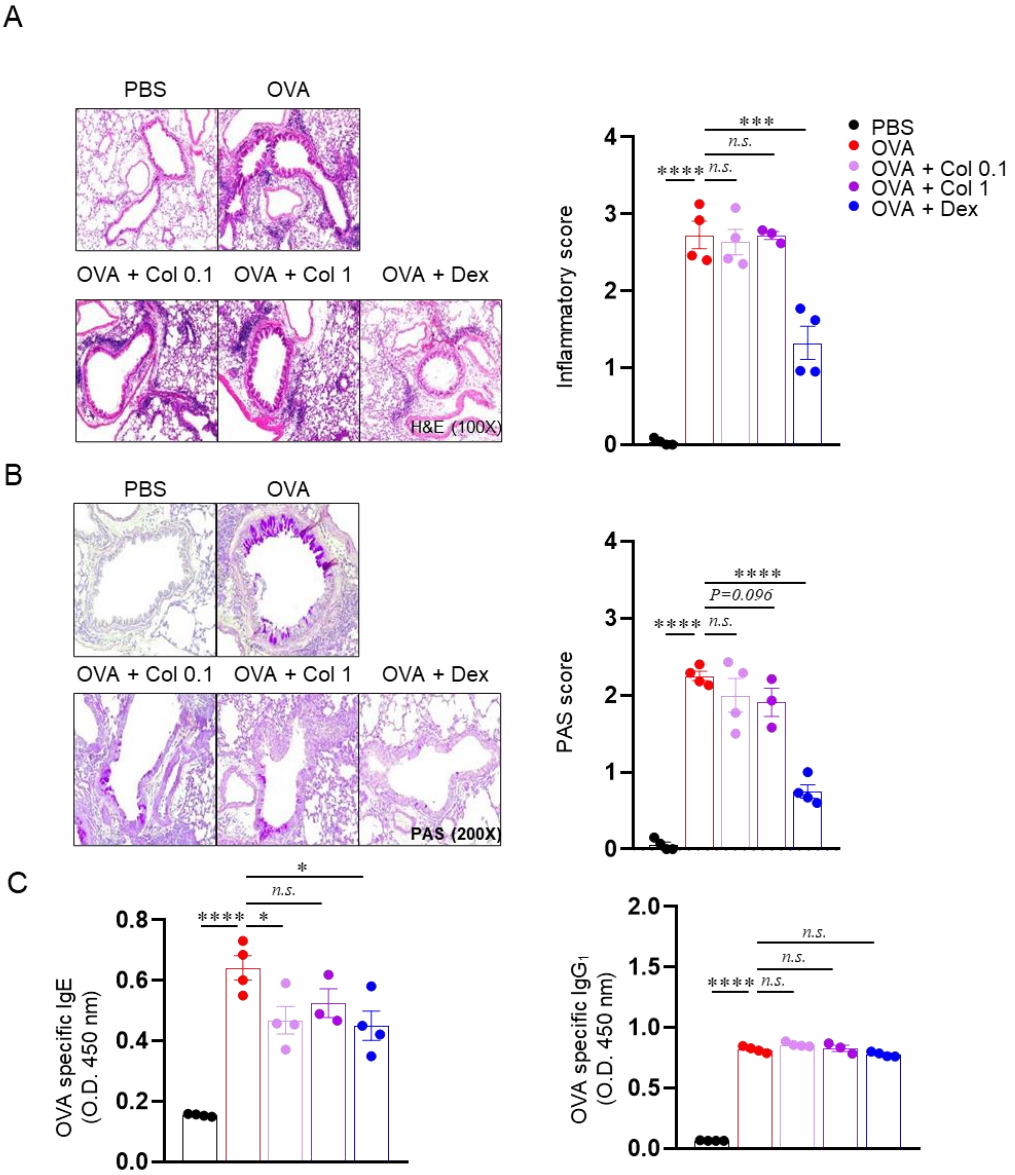

Figure 6. The effect of colchicine on histological analysis and serum levels of OVA specific IgE and IgG_1 on mouse model of asthma. Histological analysis included **(A)** H&E staining for scoring inflammatory responses and **(B)** PAS staining for detecting

mucus accumulation in lung tissues. The scoring were conducted by semiquantitative scoring system.[72] **(C)** The serum levels of IgE and IgG_1 in the mouse blood serum were detected by ELISA. Data are means ± SEM. Statistical analysis was conducted by unpaired *t-test*. ***$p < .001$, ****$p < .0001$, and *n.s.*: not significant.

3.6. Colchicine treatment decreased the production of cytokine in the Lung and BAL fluids of OVA induced asthma mouse model

We evaluated cytokine production of IL-5, IL-13, IL-17AF, and IFN-γ in BALF. Type 2 cytokine enhances the lung eosinophilia, mucus production and AHR following airway inflammation. IL-5 level was slightly lower in colchicine treatment group, but the difference was not statistically significant **(Figure.7A)**. However, colchicine 1 mg/kg treatment group had significantly lower levels of IL-13 than OVA challenged mice group **(Figure.7B)**. And eotaxin levels was slightly lower in colchicine treatment group **(Figure. 7C)**. IL-17AF and IFN- γ were not significantly different between colchicine treatments group and OVA challenged mice group **(Figure.7D)**. These results show that colchicine decreased Th2 cytokine level especially IL-13 and suggest that colchicine regulate the cytokine secretion that play important roles in inflammatory cell infiltration. We then confirmed Th2 cytokine production of IL-5, IL-13 in lung re-stimulated by OVA. Tissue-resident memory Th2 cells are important cells to orchestrate local Th2 cell immunity.[75] To examine the activation of tissue-resident memory Th2 cells, we measured Th2 cytokine levels by ELISA. IL-5 level was significantly decreased in colchicine treatment group. Similarly, IL-13 level was also decreased in colchicine group. IL-17AF and IFN- γ level were not detected. These results show that colchicine decreased IL-5, IL-13 cytokine levels produced by lung and suggest that colchicine regulate the cytokine production by tissue-resident memory Th2 cells in lung.

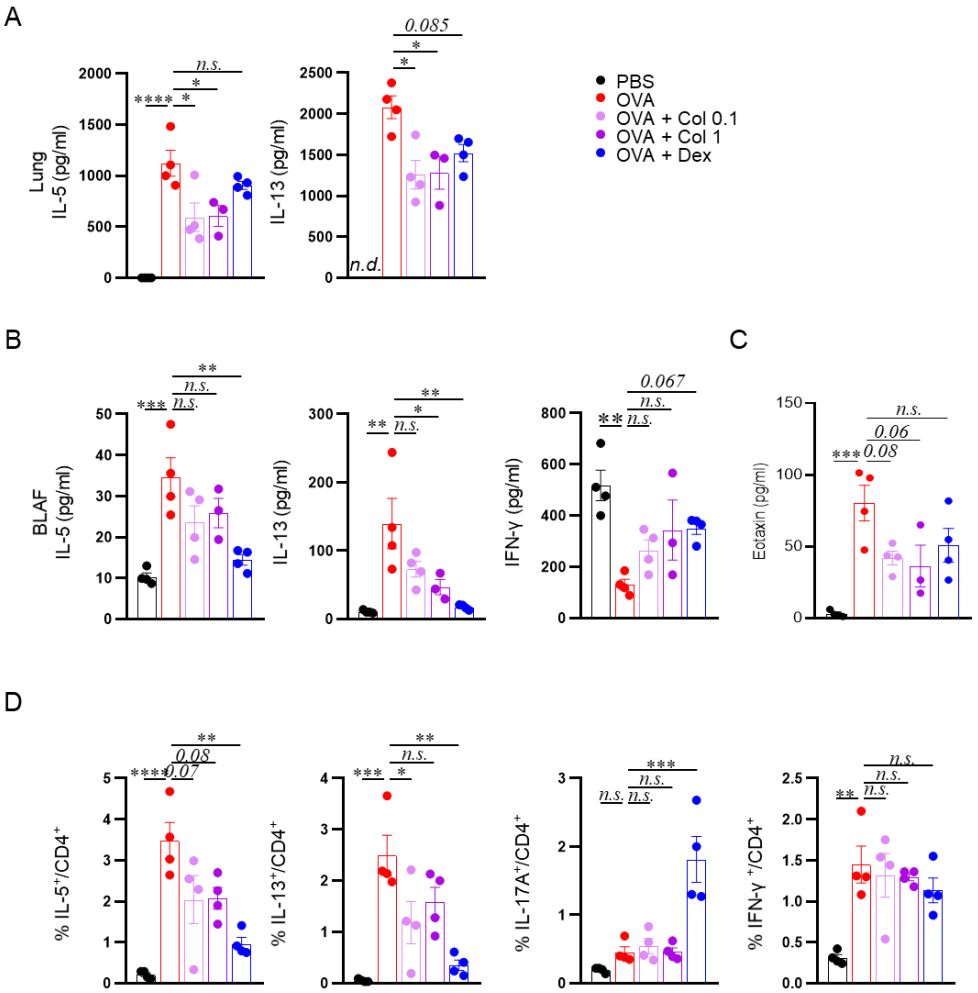

Figure 7. The cytokine levels of BALF after colchicine treatment on mouse model of asthma. (A) The level of Th2 cytokine IL-5, IL-13 in Lung were measured by ELISA. **(B)** The level of cytokine IL-5, IL-13, IL-17AF, IFN-γ and **(C)** chemokine Eotaxin in BALF were measured by ELISA. **(D)** The cytokine level were detected by flow cytometry. Data are means ± SEM. Statistical analysis was conducted by one-way ANOVA with Tukey's multiple comparisons test. *$p < .05$, **$p < .01$ ***$p < .001$, ****$p < .0001$, and *n.s.*: not significant.

4. Discussion

In this study, we explored the distinct immunoregulatory effects of NOX4 deficiency and colchicine treatment in asthma mouse model. Our findings show that while NOX4 deficiency reduced airway inflammation and mucus hypersecretion, it did not significantly affect Th2 cytokine production or eosinophilic infiltration. Conversely, colchicine treatment suppressed IL-4 and IL-13 secretion and reduced eosinophil accumulation both *in vitro* and *in vivo*, yet had limited impact on histological improvement. These results suggest that NOX4 and colchicine modulate distinct aspects of immune responses and tissue pathology in asthma. Histologically, colchicine showed only modest effects, whereas NOX4 deficiency resulted in more evident improvement.

Previous studies have demonstrated that NOX4, a member of the NADPH oxidase family, plays a pivotal role in asthma-related oxidative stress and tissue remodeling. It has been shown that NOX4 is upregulated in asthmatic airways, and its inhibition attenuates airway fibrosis and inflammation in OVA-induced models.[76] Our findings are consistent with this, showing reduced inflammation and mucus production in *Nox4*$^{-/-}$ mice, which may possibly be associated with attenuated TGF-β1/Smad signaling, although this mechanism was not directly examined in our study. Interestingly, Th2 cytokine levels remained unchanged, suggesting that NOX4 may influence disease progression primarily via effects on structural cells rather than adaptive immune cells. Supporting this, recent evidence has shown that microRNA-based suppression of NOX4 can reduce IL-4, IL-5, and IL-13 expression while ameliorating histopathological changes in asthmatic mice.[77] Together, these data indicate that NOX4 inhibition may preferentially target epithelial inflammation and remodeling without broadly suppressing Th2 immunity.

Colchicine, a known microtubule inhibitor and nonsteroidal anti-inflammatory agent, exerts immunomodulatory effects by interfering with cell motility, trafficking, and cytokine secretion. By inhibiting the NLRP3 inflammasome, it also affects the functional properties of dendritic and T cells.[78] Clinically, colchicine enhances regulatory T cell activity and reduces serum IgE levels in allergic conditions.[79] In our study, colchicine significantly downregulated IL-4 and IL-13 production from activated splenic $CD4^+$ T cells and decreased eosinophilic infiltration in the lungs and bronchoalveolar lavage fluid. However, histopathological assessment revealed minimal changes, indicating that suppression of Th2 cytokines alone may not be sufficient to reverse established airway remodeling. This observation is supported by clinical trials targeting IL-5 and IL-13, which, despite reducing eosinophil numbers, failed to produce consistent improvements in lung function or tissue histology.[80]

The persistence of airway pathology despite cytokine reduction may reflect contributions from alternative inflammatory pathways. Cytokines such as IL-33 and IL-25, along with epithelial-derived growth factors like TGF-β, are known to contribute to airway remodeling independently of Th2 activity. It is plausible that colchicine does not sufficiently inhibit these pathways, while NOX4 inhibition may affect them indirectly through the modulation of epithelial ROS signaling and autophagy-associated cytokine release.[81] Thus, NOX4 and colchicine target complementary arms of the asthma inflammatory cascade NOX4 predominantly modulating structural and innate responses, and colchicine targeting adaptive Th2-mediated inflammation.

Altogether, our data suggest that while NOX4 deficiency and colchicine monotherapy each confer partial protective effects, neither fully resolves the immunopathological features of asthma. NOX4 deletion mitigates airway remodeling and tissue inflammation, whereas colchicine curtails Th2-driven cytokine production and eosinophil infiltration. The lack of complete efficacy from either strategy alone highlights the complexity of asthma pathogenesis, underscoring the potential benefit of dual-targeted therapy. A combined approach targeting oxidative stress pathways and microtubule-dependent immune cell function may offer enhanced control of both inflammation and structural damage. Future investigations should assess the therapeutic synergy of NOX4 inhibitors and colchicine in chronic asthma models, as well as their effects on epithelial integrity and long-term airway function. Mechanistic studies are also needed to delineate the cross-talk between epithelial, stromal, and immune compartments under dual-pathway modulation.

5. Conclusion

This study highlights the differential yet complementary roles of NOX4 inhibition and colchicine treatment in modulating asthma-related inflammation. NOX4 deficiency primarily reduced airway remodeling and epithelial inflammation without significantly altering Th2 cytokine levels. In contrast, colchicine effectively suppressed IL-5 and IL-13 production and reduced eosinophil infiltration, but did not lead to substantial improvements in lung histopathology. These findings underscore the complexity of asthma pathogenesis, wherein structural and immunological pathways operate in parallel. Targeting a single pathway may only partially mitigate disease severity. Therefore, a combinatorial approach that concurrently inhibits oxidative signaling and Th2-mediated immune activation may offer superior therapeutic benefits. Future studies are warranted to explore this dual-targeted strategy in chronic asthma models and to assess its long-term efficacy in restoring airway function and integrity.

References

1. World Health Organization. *Global Tuberculosis Report 2024*. Geneva: World Health Organization; 2024; 1–68.
2. Young C, Walzl G, Du Plessis N. Therapeutic host-directed strategies to improve outcome in tuberculosis. *Mucosal Immunol* 2020;13:190-204.
3. Choi E, Choi HH, Kwon KW, Kim H, Ryu JH, Hong JJ, et al. Permissive lung neutrophils facilitate tuberculosis immunopathogenesis in male phagocyte NADPH oxidase-deficient mice. *PLoS Pathog* 2024;20:e1012500.
4. Olive AJ, Smith CM, Kiritsy MC, Sassetti CM. The phagocyte oxidase controls tolerance to *Mycobacterium tuberculosis* infection. *J Immunol* 2018;201:1705-16.
5. Han S, Moon S, Chung YW, Ryu JH. NADPH Oxidase 4-mediated alveolar macrophage recruitment to lung attenuates neutrophilic inflammation in *Staphylococcus aureus* infection. *Immune Netw* 2023;23:e42.
6. Thapa J, Yoshiiri G, Ito K, Okubo T, Nakamura S, Furuta Y, et al. *Chlamydia trachomatis* requires functional host-cell mitochondria and NADPH oxidase 4/p38MAPK signaling for growth in normoxia. *Front Cell Infect Microbiol* 2022;12:902492.
7. Hendricks KS, To EE, Luong R, Liong F, Erlich JR, Shah AM, et al. Endothelial NOX4 oxidase negatively regulates inflammation and improves morbidity during influenza A virus lung infection in mice. *Front Cell Infect Microbiol* 2022;12:883448.
8. Kim JH, Lee J, Bae SJ, Kim Y, Park BJ, Choi JW, et al. NADPH oxidase 4 is required for the generation of macrophage migration inhibitory factor and host defense against *Toxoplasma gondii* infection. *Sci Rep* 2017;7:6361.
9. Dolowschiak T, Chassin C, Ben Mkaddem S, Fuchs TM, Weiss S, Vandewalle A, et al. Potentiation of epithelial innate host responses by intercellular communication. *PLoS Pathog* 2010;6:e1001194.
10. Hecker L, Logsdon NJ, Kurundkar D, Kurundkar A, Bernard K, Hock T, et al.

Reversal of persistent fibrosis in aging by targeting Nox4-Nrf2 redox imbalance. *Sci Transl Med* 2014;6:231ra47.

11. Woo SJ, Kim Y, Jung H, Lee JJ, Hong JY. MicroRNA 148a suppresses tuberculous fibrosis by targeting NOX4 and POLDIP2. *Int J Mol Sci* 2022;23.
12. Woo SJ, Kim Y, Jung H, Lee JJ, Hong JY. Tuberculous fibrosis enhances tumorigenic potential via the NOX4-autophagy axis. *Cancers (Basel)* 2021;13.
13. Kim Y, Park SY, Jung H, Noh YS, Lee JJ, Hong JY. Inhibition of NADPH oxidase 4 (NOX4) signaling attenuates tuberculous pleural fibrosis. *J Clin Med* 2019;8.
14. Mihret A. The role of dendritic cells in *Mycobacterium tuberculosis* infection. *Virulence* 2012;3:654-9.
15. Hossain MM, Norazmi MN. Pattern recognition receptors and cytokines in Mycobacterium tuberculosis infection--the double-edged sword? *Biomed Res Int* 2013;2013:179174.
16. Domingo-Gonzalez R, Prince O, Cooper A, Khader SA. Cytokines and chemokines in *Mycobacterium tuberculosis* infection. *Microbiol Spectr* 2016;4.
17. Mihret A, Mamo G, Tafesse M, Hailu A, Parida S. Dendritic cells activate and mature after infection with *Mycobacterium tuberculosis*. *BMC Res Notes* 2011;4:247.
18. Bafica A, Scanga CA, Feng CG, Leifer C, Cheever A, Sher A. TLR9 regulates Th1 responses and cooperates with TLR2 in mediating optimal resistance to *Mycobacterium tuberculosis*. *J Exp Med* 2005;202:1715-24.
19. Lyadova IV, Panteleev AV. Th1 and Th17 cells in tuberculosis: protection, pathology, and biomarkers. *Mediators Inflamm* 2015;2015:854507.
20. Vignali DA, Kuchroo VK. IL-12 family cytokines: immunological playmakers. *Nat Immunol* 2012;13:722-8.
21. Gallegos AM, van Heijst JW, Samstein M, Su X, Pamer EG, Glickman MS. A gamma interferon independent mechanism of CD4 T cell mediated control of *M. tuberculosis* infection *in vivo*. *PLoS Pathog* 2011;7:e1002052.

22. Helfinger V, Palfi K, Weigert A, Schroder K. The NADPH oxidase Nox4 controls macrophage polarization in an NFkappaB-dependent manner. *Oxid Med Cell Longev* 2019;2019:3264858.
23. Zhang J, Li H, Wu Q, Chen Y, Deng Y, Yang Z, et al. Tumoral NOX4 recruits M2 tumor-associated macrophages via ROS/PI3K signaling-dependent various cytokine production to promote NSCLC growth. *Redox Biol* 2019;22:101116.
24. Lee SR, Lee HE, Yoo JY, An EJ, Song SJ, Han KH, et al. Nox4-SH3YL1 complex is involved in diabetic nephropathy. *iScience* 2024;27:108868.
25. Lee JH, Joo JH, Kim J, Lim HJ, Kim S, Curtiss L, et al. Interaction of NADPH oxidase 1 with Toll-like receptor 2 induces migration of smooth muscle cells. *Cardiovasc Res* 2013;99:483-93.
26. Jeon BY, Kwak J, Hahn MY, Eum SY, Yang J, Kim SC, et al. *In vivo* characteristics of Korean Beijing *Mycobacterium tuberculosis* strain K1 in an aerosol challenge model and in the Cornell latent tuberculosis model. *J Med Microbiol* 2012;61:1373-9.
27. Kwon KW, Choi HH, Han SJ, Kim JS, Kim WS, Kim H, et al. Vaccine efficacy of a *Mycobacterium tuberculosis* Beijing-specific proline-glutamic acid (PE) antigen against highly virulent outbreak isolates. *FASEB J* 2019;33:6483-96.
28. Kim H, Song EJ, Choi E, Kwon KW, Park JH, Shin SJ. Adjunctive administration of parabiotic *Lactobacillus sakei* CVL-001 ameliorates drug-induced toxicity and pulmonary inflammation during antibiotic treatment for tuberculosis. *Int Immunopharmacol* 2024;132:111937.
29. Kang TG, Kwon KW, Kim K, Lee I, Kim MJ, Ha SJ, et al. Viral coinfection promotes tuberculosis immunopathogenesis by type I IFN signaling-dependent impediment of Th1 cell pulmonary influx. *Nat Commun* 2022;13:3155.
30. Lee JM, Park J, Reed SG, Coler RN, Hong JJ, Kim LH, et al. Vaccination inducing durable and robust antigen-specific Th1/Th17 immune responses contributes to prophylactic protection against *Mycobacterium avium* infection but is ineffective

as an adjunct to antibiotic treatment in chronic disease. *Virulence* 2022;13:808-32.

31. Choi HG, Kwon KW, Choi S, Back YW, Park HS, Kang SM, et al. Antigen-specific IFN-gamma/IL-17-co-producing $CD4^+$ T-cells are the determinants for protective efficacy of tuberculosis subunit vaccine. *Vaccines (Basel)* 2020;8.
32. Choi HH, Kwon KW, Han SJ, Kang SM, Choi E, Kim A, et al. PPE39 of the *Mycobacterium tuberculosis* strain Beijing/K induces Th1-cell polarization through dendritic cell maturation. *J Cell Sci* 2019;132.
33. Kolloli A, Kumar R, Venketaraman V, Subbian S. Immunopathology of pulmonary *Mycobacterium tuberculosis* infection in a humanized mouse model. *Int J Mol Sci* 2024;25.
34. Chackerian AA, Alt JM, Perera TV, Dascher CC, Behar SM. Dissemination of *Mycobacterium tuberculosis* is influenced by host factors and precedes the initiation of T-cell immunity. *Infect Immun* 2002;70:4501-9.
35. Garvin AJ, Khalaf AHA, Rettino A, Xicluna J, Butler L, Morris JR, et al. GSK3beta-SCFFBXW7alpha mediated phosphorylation and ubiquitination of IRF1 are required for its transcription-dependent turnover. *Nucleic Acids Res* 2019;47:4476-94.
36. Gautier G, Humbert M, Deauvieau F, Scuiller M, Hiscott J, Bates EE, et al. A type I interferon autocrine-paracrine loop is involved in Toll-like receptor-induced interleukin-12p70 secretion by dendritic cells. *J Exp Med* 2005;201:1435-46.
37. Davies LRL, Wang C, Steigler P, Bowman KA, Fischinger S, Hatherill M, et al. Age and sex influence antibody profiles associated with tuberculosis progression. *Nat Microbiol* 2024;9:1513-25.
38. Gupta M, Srikrishna G, Klein SL, Bishai WR. Genetic and hormonal mechanisms underlying sex-specific immune responses in tuberculosis. *Trends Immunol* 2022;43:640-56.
39. Marcoa R, Ribeiro AI, Zao I, Duarte R. Tuberculosis and gender - factors influencing the risk of tuberculosis among men and women by age group.

Pulmonology 2018;24:199-202.

40. Zhou X, Xu H, Li Q, Wang Q, Liu H, Huang Y, et al. Viperin deficiency promotes dendritic cell activation and function via NF-kappaB activation during *Mycobacterium tuberculosis* infection. *Inflamm Res* 2023;72:27-41.
41. Orme IM, Roberts AD, Griffin JP, Abrams JS. Cytokine secretion by CD4 T lymphocytes acquired in response to *Mycobacterium tuberculosis* infection. J Immunol 1993;151:518-25.
42. Shimokata K, Kishimoto H, Takagi E, Tsunekawa H. Determination of the T-cell subset producing gamma-interferon in tuberculous pleural effusion. *Microbiol Immunol* 1986;30:353-61.
43. Su H, Peng B, Zhang Z, Liu Z, Zhang Z. The *Mycobacterium tuberculosis* glycoprotein Rv1016c protein inhibits dendritic cell maturation, and impairs Th1 /Th17 responses during mycobacteria infection. *Mol Immunol* 2019;109:58-70.
44. Cooper AM, Solache A, Khader SA. Interleukin-12 and tuberculosis: an old story revisited. *Curr Opin Immunol* 2007;19:441-7.
45. Yoeli-Lerner M, Chin YR, Hansen CK, Toker A. Akt/protein kinase b and glycogen synthase kinase-3beta signaling pathway regulates cell migration through the NFAT1 transcription factor. *Mol Cancer Res* 2009;7:425-32.
46. Rodionova E, Conzelmann M, Maraskovsky E, Hess M, Kirsch M, Giese T, et al. GSK-3 mediates differentiation and activation of proinflammatory dendritic cells. *Blood* 2007;109:1584-92.
47. Kim J, Kim J, Lim HJ, Lee S, Bae YS, Kim J. Nox4-IGF2 axis promotes differentiation of embryoid body cells into derivatives of the three embryonic germ layers. S*tem Cell Rev Rep* 2022;18:1181-92.
48. Yoshikawa Y, Ago T, Kuroda J, Wakisaka Y, Tachibana M, Komori M, et al. Nox4 promotes neural stem/Precursor cell proliferation and neurogenesis in the hippocampus and restores memory function following trimethyltin-induced injury. *Neuroscience* 2019;398:193-205.

49. Zhou M, Zhao X, Liao L, Deng Y, Liu M, Wang J, et al. Forsythiaside a regulates activation of hepatic stellate cells by inhibiting NOX4-dependent ROS. *Oxid Med Cell Longev* 2022;2022:9938392.
50. Zhang C, Lan T, Hou J, Li J, Fang R, Yang Z, et al. NOX4 promotes non-small cell lung cancer cell proliferation and metastasis through positive feedback regulation of PI3K/Akt signaling. *Oncotarget* 2014;5:4392-405
51. Lee CF, Qiao M, Schroder K, Zhao Q, Asmis R. Nox4 is a novel inducible source of reactive oxygen species in monocytes and macrophages and mediates oxidized low density lipoprotein-induced macrophage death. Circ Res 2010;106:1489-97.
52. Braman SS. The global burden of asthma. *Chest* 2006;130:4S-12S.
53. Fedorov VD, Shelygin YA. Treatment of patients with rectal cancer. *Dis Colon Rectum* 1989;32:138-45.
54. Richter A, Myhre B, Khanna SC. An automated apparatus for dissolution studies. *J Pharm Pharmacol* 1969;21:409-14.
55. Sandmann B, Happ B, Kupfer S, Schacher FH, Hager MD, Schubert US. The self-healing potential of triazole-pyridine-based metallopolymers. *Macromol Rapid Commun* 2015;36:604-9.
56. Wills-Karp M. Interleukin-13 in asthma pathogenesis. *Immunol Rev* 2004;202:175-90.
57. Kruse RL, Vanijcharoenkarn K. Drug repurposing to treat asthma and allergic disorders: Progress and prospects. *Allergy* 2018;73:313-22.
58. 17th annual UCLA symposium. Abstracts: Metal ion homeostasis: molecular biology and chemistry. *J Cell Biochem Suppl* 1988;12D:321-58.
59. Liu CW, Lee TL, Chen YC, Liang CJ, Wang SH, Lue JH, et al. PM(2.5)-induced oxidative stress increases intercellular adhesion molecule-1 expression in lung epithelial cells through the IL-6/AKT/STAT3/NF-kappaB-dependent pathway. *Part Fibre Toxicol* 2018;15:4.
60. Zhao QD, Viswanadhapalli S, Williams P, Shi Q, Tan C, Yi X, et al. NADPH

oxidase 4 induces cardiac fibrosis and hypertrophy through activating Akt/mTOR and NFkappaB signaling pathways. *Circulation* 2015;131:643-55.

61. Clissiounis N. Effect of adrenergic drugs on morphine-induced hyperglycemia. *Life Sci* 1979;25:391-4.
62. Rogozea R. Biofeedback therapy. *Neurol Psychiatr* (Bucur) 1979;17:261-8.
63. Sertkaya A, Beleche T, Jessup A, Sommers BD. Costs of Drug Development and Research and Development Intensity in the US, 2000-2018. *JAMA Netw Open* 2024;7:e2415445.
64. Stack J, Ryan J, McCarthy G. Colchicine: New Insights to an Old Drug. *Am J Ther* 2015;22:e151-7.
65. Angelidis C, Kotsialou Z, Kossyvakis C, Vrettou AR, Zacharoulis A, Kolokathis F, et al. Colchicine Pharmacokinetics and Mechanism of Action. *Curr Pharm Des* 2018;24:659-63.
66. Dalbeth N, Lauterio TJ, Wolfe HR. Mechanism of action of colchicine in the treatment of gout. *Clin Ther* 2014;36:1465-79.
67. Ghaith HS, Gabra MD, Nafady MH, Elshawah HE, Negida A, Mushtaq G, et al. A Review of the Rational and Current Evidence on Colchicine for COVID-19. *Curr Pharm Des* 2022;28:3194-201.
68. Kofler T, Kurmann R, Lehnick D, Cioffi GM, Chandran S, Attinger-Toller A, et al. Colchicine in Patients With Coronary Artery Disease: A Systematic Review and Meta-Analysis of Randomized Trials. *J Am Heart Assoc* 2021;10:e021198.
69. Kwon KW, Kim LH, Kang SM, Lee JM, Choi E, Park J, et al. Host-directed anti-mycobacterial activity of colchicine, an anti-gout drug, via strengthened host innate resistance reinforced by the IL-1beta/PGE(2) axis. *Br J Pharmacol* 2022;179:3951-69.
70. Zhao Y, Shen QR, Chen YX, Shi Y, Wu WB, Li Q, et al. Colchicine protects against the development of experimental abdominal aortic aneurysm. *Clin Sci* (Lond) 2023;137:1533-45.

71. Park SC, Kim H, Bak Y, Shim D, Kwon KW, Kim CH, et al. An Alternative Dendritic Cell-Induced Murine Model of Asthma Exhibiting a Robust Th2/Th17-Skewed Response. *Allergy Asthma Immunol Res* 2020;12:537-55.
72. Yoshioka M, Sagara H, Takahashi F, Harada N, Nishio K, Mori A, et al. Role of multidrug resistance-associated protein 1 in the pathogenesis of allergic airway inflammation. *Am J Physiol Lung Cell Mol Physiol* 2009;296:L30-6.
73. Perico N, Ostermann D, Bontempeill M, Morigi M, Amuchastegui CS, Zoja C, et al. Colchicine interferes with L-selectin and leukocyte function-associated antigen-1 expression on human T lymphocytes and inhibits T cell activation. *J Am Soc Nephrol* 1996;7:594-601.
74. Davoine F, Lacy P. Eosinophil cytokines, chemokines, and growth factors: emerging roles in immunity. *Front Immunol* 2014;5:570.
75. Andrea M, Susanna B, Francesca N, Enrico M, Alessandra V. The emerging role of type 2 inflammation in asthma. *Expert Rev Clin Immunol* 2021;17:63-71.
76. Zhao H, Shan J, Peng L, Yu H. Adaptive Event-Triggered Bipartite Formation for Multiagent Systems via Reinforcement Learning. *IEEE Trans Neural Netw Learn Syst* 2024;35:17817-28.
77. Yang R, Zheng K, Wu B, Li D, Wang Z, Wang X. Predicting User Susceptibility to Phishing Based on Multidimensional Features. *Comput Intell Neurosci* 2022;2022:7058972.
78. Dubessy AL, Zujovic V, Papeix C, Stankoff B. Biotherapies in multiple sclerosis: a step toward remyelination and neuroprotection? *Rev Neurol* (Paris) 2014;170:770-8.
79. Trump DL, Ravdin PM, Borden EC, Magers CF, Whisnant JK. Interferon-alpha-n1 and continuous infusion vinblastine for treatment of advanced renal cell carcinoma. *J Biol Response Mod* 1990;9:108-11.
80. He X, Zeng X, Troendle J, Ahlberg M, Tilden EL, Souza JP, et al. New insights on labor progression: a systematic review. *Am J Obstet Gynecol* 2023;228:S1063-S94.

81. Heavner SF, Anderson W, Kashyap R, Dasher P, Mathe EA, Merson L, et al. A Path to Real-World Evidence in Critical Care Using Open-Source Data Harmonization Tools. *Crit Care Explor* 2023;5:e0893.

Abstract in Korean

다양한 만성 폐질환에서의 면역조절 기전에 대한 분석 연구

결핵(TB)과 천식과 같은 만성 폐질환은 구조 세포와 면역세포 간의 복잡한 상호작용에 의해 매개되는 만성 염증을 특징으로 한다. 다양한 면역 경로를 표적으로 하는 면역 조절 접근법은 질환 완화의 가능성을 제공할 수 있으며, 만성 염증을 효과적으로 조절하고 조직 손상을 최소화하는 전략은 이러한 폐질환을 관리하는 데 필수적이다. 본 연구에서는 서로 다른 폐질환 마우스 모델을 활용하여 면역 조절 기전을 탐색하였다. 첫 번째 모델은 NADPH oxidase 계열의 구성원인 NOX4 가 결핵 감염과 천식에서 면역 반응을 어떻게 조절하는지를 평가하였고, 두 번째 모델에서는 항염증 효과로 알려진 콜히친(colchicine)이 천식에서 적응 면역 기전에 영향을 줄 수 있는지를 분석하였다.

결핵 마우스 모델에서 NOX4 결핍은 폐 내 세균 부하 감소 및 염증 완화와 연관되었으며, *Nox4*$^{-/-}$ 마우스에서는 수지상세포(DC)의 침윤과 IFN-ɣ 를 분비하는 $CD4^+$ T 세포의 비율이 증가하였다. 기전적으로, *Nox4*$^{-/-}$ 유래 DC 는 AKT/GSK-3β 경로를 통한 IRF1 활성화에 의해 IL-12 발현이 증가하였고, 이로 인해 Th1 분화가 촉진되어 효과적인 Mtb 면역 조절이 유도되었다. 또한 Bacillus Calmette-Guérin(BCG) 백신은 $Nox4^{-/-}$ 마우스에서 더 효과적으로 작용하였으며, 이는 NOX4 가 결핵 감염에서 보호 면역을 음성적으로 조절함을 시사하며, 백신 보조제 타깃으로서의 가능성을 나타낸다.

한편 천식 모델에서는 NOX4 결핍이 기관지 염증 및 점액 생성은 완화하였지만, Th2 사이토카인 수치나 호산구 유입에는 유의미한 영향을 주지 않았다. 반면 콜히친은 자극된 $CD4^+$ T 세포에서 IL-4 및 IL-13 분비를 유의미하게 억제하였고, 폐조직과 기관지폐포세척액(BALF) 모두에서 호산구 침윤을 현저히 감소시켰다. 그러나 콜히친은 이미 형성된 조직 병리학적 변화에는 뚜렷한 개선 효과를 보이지 않았으며, 이는 사이토카인 조절과 조직 재형성 간의 분리 가능성을 시사한다. 이러한 결과는 효과적인 천식 조절을 위해서는 선천 면역 경로와 적응 면역 경로를 동시에 표적으로 삼는 전략이 필요함을 강조한다.

종합적으로, 본 연구는 NOX4 가 결핵과 천식이라는 서로 다른 폐질환 환경에서 선천면역세포 기능과 조직 염증을 조절한다는 점을 보여준다. 반면, 콜히친은 Th2 매개 사이토카인 반응에 선택적으로 작용하였으나 구조적 병리 개선에는 제한적인 효과를 보였다. 이와 같은 결과는 산화 스트레스를 조절하고 콜히친과 같은 비스테로이드성 항염증제를 대안적 접근법으로 탐색하는 것이 만성 폐질환의 치료 가능성을 제시할 수 있음을 시사한다. 특히, 면역 반응을 조절하여 염증을 완화하는 접근은 효과적인 치료 옵션이 될 수 있으며, 이 과정에서 NOX4 는 유망한 면역조절 표적으로 작용할 가능성이 있다.

핵심되는 말: 결핵, 천식, NADPH 산화효소 4(NOX4), 콜히친, 제1형 보조 T 세포, 호산구, 제2형 보조 T 세포